Miner Deposita (2009) 44:723–750
DOI 10.1007/s00126-009-0240-8

ARTICLE

The Kenticha rare-element pegmatite, Ethiopia: internal differentiation, U–Pb age and Ta mineralization

Dirk Küster · Rolf L. Romer · Dandena Tolessa · Desta Zerihun · K. Bheemalingeswara · Frank Melcher · Thomas Oberthür

Received: 11 June 2008 / Accepted: 20 March 2009 / Published online: 22 April 2009

Abstract The Kenticha rare-element pegmatite, a globally important tantalite source in the Neoproterozoic Adola Belt of southern Ethiopia, is a highly fractionated, huge (2,000 m long and up to 100 m thick), subhorizontal, sheet-like body, discordantly emplaced in ultramafic host rock. It corresponds to the spodumene subtype of the rare-element pegmatite class and belongs to the lithium–cesium–tantalum petrogenetic family. The Kenticha pegmatite is asymmetrically zoned from bottom to top into granitic lower zone, spodumene-free intermediate zone, and spodumene-bearing upper zone. A monomineralic quartz unit is discontinuously developed within the upper zone. Whole-rock data indicate an internal geochemical differentiation of the pegmatite sheet proceeding from the lower zone (K/Rb ~36, K/Cs ~440, Al/Ga ~2,060, Nb/Ta ~2.6) to the upper zone (K/Rb ~19, K/Cs ~96, Al/Ga ~1,600, Nb/Ta ~0.7). The latter one is strongly enriched in Li_2O (up to 3.21%), Rb (up to 4,570 ppm), Cs (up to 730 ppm), Ga (up to 71 ppm), and Ta (up to 554 ppm). Similar trends of increasing fractionation from lower zone to upper zone were obtained in muscovite (K/Rb 23–14, K/Cs 580–290, K/Tl 6,790–3,730, Fe/Mn 19–10, Nb/Ta 6.5–3.8) and columbite–tantalite (Mn/Mn + Fe 0.4–1, Ta/Ta + Nb 0.1–0.9). The bottom-to-top differentiation of the Kenticha pegmatite and the Ta mineralization in its upper part are principally attributed to upward in situ fractionation of a residual leucogranitic to pegmatitic melt, largely under closed system conditions. High MgO contents (up to 5.05%) in parts of the upper zone are the result of postmagmatic hydrothermal alteration and contamination by hanging wall serpentinite. U–Pb dating of Mn-tantalite from two zones of the Kenticha pegmatite gave ages of 530.2±1.3 and 530.0±2.3 Ma. Mn-tantalite from the Bupo pegmatite, situated 9 km north of Kenticha, gave an age of

Editorial handling: B. Lehmann

D. Küster · K. Bheemalingeswara
Department of Applied Geology, Mekelle University,
P.O. Box 231 Mekelle, Ethiopia

D. Küster (✉)
Institut für Angewandte Geowissenschaften,
Technische Universität Berlin,
FG Mineralogie-Petrologie Ackerstrasse 71–76,
13355 Berlin, Germany
e-mail: Dirk.Kuester@bgr.de

R. L. Romer
GeoForschungsZentrum Potsdam,
Telegrafenberg,
14473 Potsdam, Germany

D. Tolessa
Geological Survey of Ethiopia,
P.O. Box 2302, Addis Ababa, Ethiopia

D. Zerihun
Ethiopian Mineral Development Share Company,
P.O. Box 2543, Addis Ababa, Ethiopia

F. Melcher · T. Oberthür
Bundesanstalt für Geowissenschaften und Rohstoffe,
Stilleweg 2,
30655 Hannover, Germany

Present Address:
D. Küster
Bundesanstalt für Geowissenschaften und Rohstoffe,
Stilleweg 2,
30655 Hannover, Germany

529.2±4.1 Ma, indicating coeval emplacement of the two pegmatites. The emplacement of the pegmatites is temporally related to postorogenic granite magmatism, producing slightly peraluminous, I-type plutons in the area surrounding the Kenticha pegmatite field. Fractionated members of this suite might be envisaged as potential parental magmas.

Keywords Ethiopia · Kenticha · Rare-element pegmatite · Muscovite chemistry · U–Pb tantalite dating · Ta mineralization

Introduction

Tantalum is a key metal in the modern electronics industry. The most important raw material source of this metal are rare-element granitic pegmatites and, to a lesser extent, pegmatite-derived residual and alluvial placer deposits. Tantalum concentrates are mainly composed of columbite–tantalite $(Fe,Mn)(Ta,Nb)_2O_6$ and small amounts of other, less common Ta oxides (e.g., microlite, ixiolite, wodginite). The ore concentrates typically contain contents of between 10% to 60% Ta_2O_5.

The Kenticha rare-element pegmatite in southern Ethiopia represents a globally important tantalum source. The mine produces around 120 t tantalum concentrate (~55% Ta_2O_5) annually and ranks among the biggest individual producers of tantalum ore worldwide. The Kenticha tantalum deposit was discovered in the 1980s in course of Ethio-Soviet exploration of the gold-bearing Adola Belt in southern Ethiopia (Kozyrev et al. 1982). During this exploration program, several rare-element pegmatites were discovered and geologically evaluated (Emelyanov et al. 1986; Poletayev et al. 1991). One of these pegmatites, the so-called main Kenticha pegmatite has been worked since the early 1990s. Up to now, tantalite mining has focused on the deeply weathered pegmatite regolith. Grade and tonnage of the hard rock tantalum potential is unknown. Ongoing exploration by the mining company (Ethiopian Mineral Development Share Company) includes drilling to assess the subsurface extent of pegmatite and tantalum mineralization.

Due to its remote location and short mining history, the Kenticha pegmatite has had little scientific study (Zerihun 1991; Zerihun et al. 1995; Tadesse and Zerihun 1996), unlike the well-known tantalum pegmatites in Australia (Greenbushes, Wodgina) or Canada (Tanco). We have carried out a whole-rock geochemical study of selected drill core samples from the Kenticha pegmatite, supplemented by mineral chemistry of muscovite and columbite–tantalite group minerals (CGM). These data sets are used to characterize the geochemical evolution and internal zonation of the Kenticha pegmatite. Furthermore, U–Pb dating of tantalite was performed to determine the age of tantalum mineralization and pegmatite emplacement, which permits the establishment of temporal relationships between mineralization, pegmatite crystallization, and various types of regional granitoid magmatism.

Geological setting

The Kenticha pegmatite is situated within the Precambrian basement of southern Ethiopia. This basement constitutes the southernmost part of the Arabian–Nubian Shield (ANS), a large segment of juvenile Neoproterozoic crust (Fig. 1) formed by accretion of oceanic arc terranes (Stoeser and Camp 1985; Stern 1994; Genna et al. 2002; Johnson and Woldehaimanot 2003). The ANS is flanked by older basement which was remobilized during the Pan-African

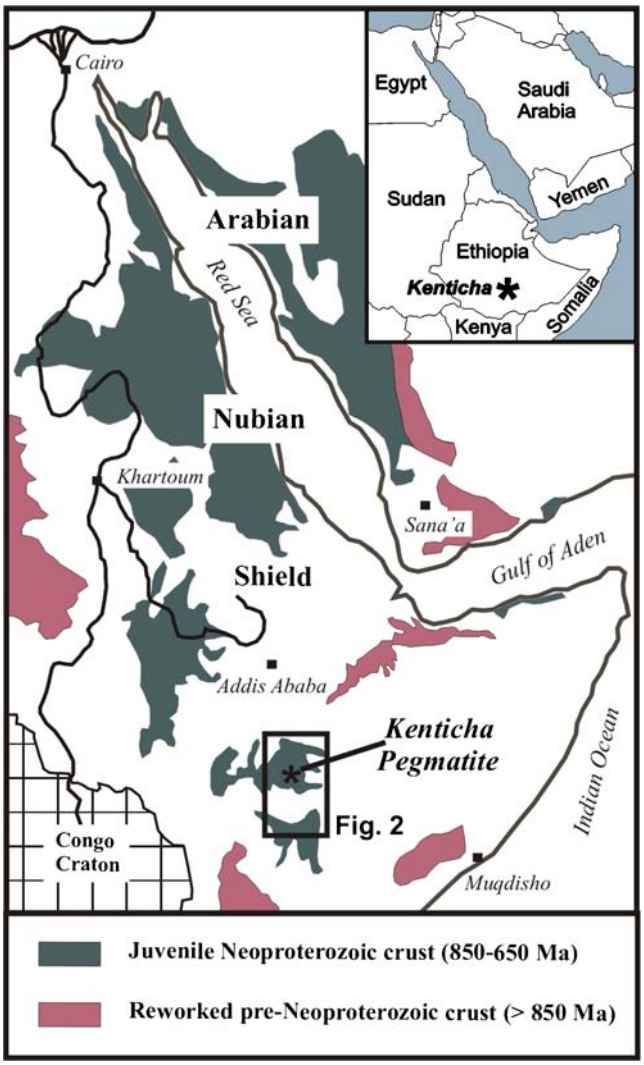

Fig. 1 Simplified geological map of northeastern Africa and location of the Kenticha pegmatite field

orogenic cycle (850–550 Ma) eventually leading to the formation of Gondwana (Fig. 1).

Tectonostratigraphy of southern Ethiopia

The Neoproterozoic rocks of southern Ethiopia are distinguished into two principal lithotectonic units: (a) granite–gneiss complexes (GGC) and (b) ophiolitic fold and thrust belts (Yibas et al. 2002). Several of these units are juxtaposed along thrust and shear zones (Fig. 2a). The high grade (amphibolite to granulite facies) GGC are composed of quartzofeldspathic, partly migmatitic para- and orthogneisses and subordinate amphibolites, and sillimanite–kyanite bearing schists. Orthogneisses and deformed batholiths of dioritic to granitic composition are abundant and are locally the dominant lithology. Based on lithological variations, Yibas et al. (2002) distinguished four granite–gneiss complexes (Adola GGC, Genale GGC, Burji-Finchaa GGC, Moyale-Sololo GGC) that are separated by major regional shear zones (Fig. 2a).

Ophiolitic fold and thrust belts (OFTB; Fig. 2a) are composed of mafic and ultramafic metavolcanic rocks and metasediments (Yibas et al. 2002). The mainly N–S to NNW–SSE striking belts have experienced low-to-medium grade (lower amphibolite facies) metamorphism. The contact of the OFTBs with the adjacent GGCs are marked by zones of multiple deformation, indicating both thrusting and strike-slip shear faulting. Yibas et al. (2002) distinguished four OFTBs: Megado, Kenticha, Bulbul, and Moyale-El Kur (Fig. 2a), differing in the chemical composition of their metabasalts (tholeiitic vs calc-alkaline, low K vs high K), the occurrence of boninitic rocks, and contrasting proportions of ultramafic and metasedimentary rocks.

Isotopic dating gave Neoproterozoic ages for both the GGCs and the OFTBs. U–Pb zircon geochronology of granitoid gneisses yielded ages between 880 and 700 Ma (Abraham et al. 1992; Genzebu et al. 1994; Worku 1996; Teklay et al. 1998; Yibas et al. 2002) which date magmatic events involved in the formation of the GGCs. Mafic magmatism in the OFTBs has been dated at 790–700 Ma (Worku 1996; Teklay et al. 1998). The GGC and OFTB units apparently form a coherent block of largely juvenile crust that probably formed in an oceanic arc setting.

Subduction-related to syncollisional granitoid magmatism, metamorphism, thrusting, and strike-slip shearing have been bracketed between 680 and 550 Ma (Beraki et al. 1989; Worku 1996; Worku and Schandelmeier 1996; Yibas et al. 2002; Yihunie 2002; Tsige and Abdelsalam 2005). These data indicate that the basement in southern Ethiopia experienced a sustained period of compressional tectonics between ca. 660 and 550 Ma. This period

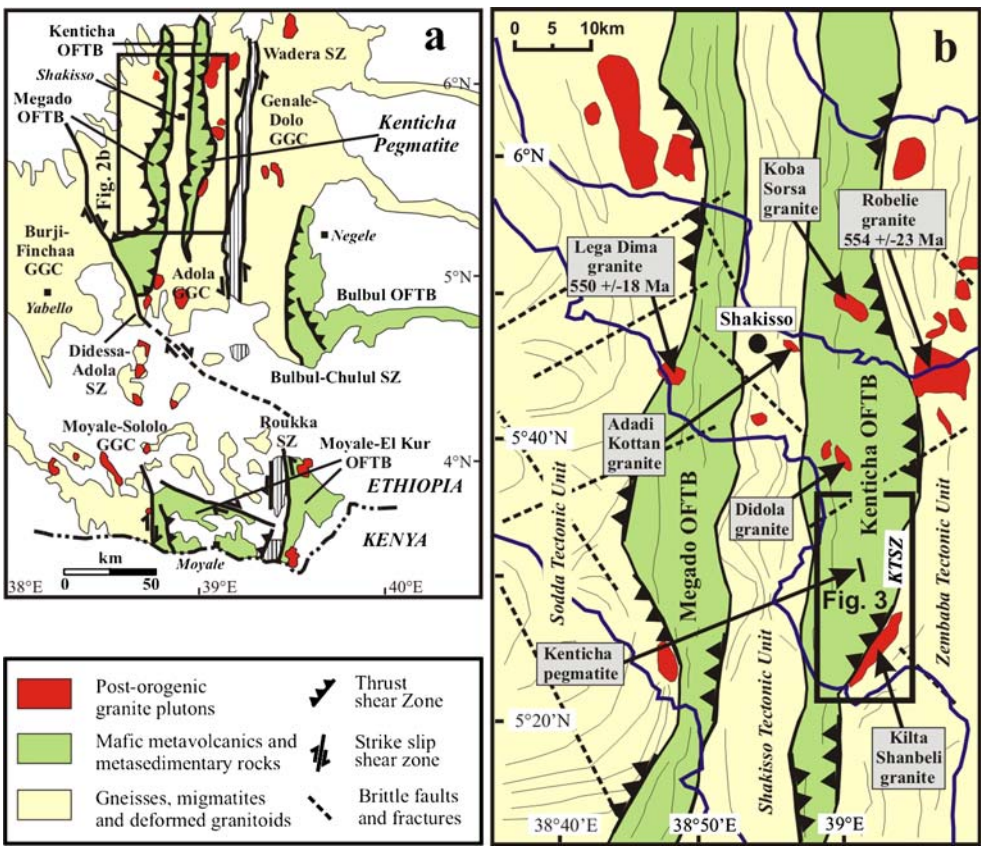

Fig. 2 Simplified geological maps of **a** southern Ethiopia (after Worku and Schandelmeier 1996; Yibas et al. 2002; Tsige and Abdelsalam 2005) and **b** the Adola Belt (simplified after Kozyrev et al. 1988; Worku and Schandelmeier 1996)

probably relates to plate convergence along a continental margin (Worku and Schandelmeier 1996).

Undeformed biotite granite plutons intruded between 550 and 520 Ma (Gichile 1991; Genzebu et al. 1994; Worku 1996; Yibas et al. 2002). These granites appear to be mainly of I-type character (Worku 1996). In the Bulbul OFTB (Fig. 2a), compressional N–S striking thrust zones were reactivated during extension-related tectonics leading to detachments along low angle normal faults (Tsige and Abdelsalam 2005).

^{40}Ar–^{39}Ar biotite and hornblende yield ages between 515 and 495 Ma (Yibas et al. 2002). Chemical Th–U–total Pb monazite and zircon ages (CHIME Isochron Method) from granites in the Kenticha and Bulbul OFTB give ages around 455 Ma (Yihunie 2003). These mineral ages probably represent isotopic resetting or new mineral growth related to anorogenic magmatic activity as described from neighboring southwestern Ethiopia (Konso pluton, Asrat and Barbey 2003) and southern Somalia (Buur granitoids, Lenoir et al. 1994).

Geology of the Adola Belt

The northwestern part of the Neoproterozoic basement of southern Ethiopia is known as the Adola Belt, collectively formed by the Adola granite–gneiss complex and two ophiolitic fold and thrust belts: the Kenticha and the Megado belt (Fig. 2b). The three lithotectonic units are juxtaposed along N–S striking thrust and shear zones. The Kenticha and Megado OFTBs are made up of greenschist to lower amphibolite facies metasediments (garnet–mica schists, graphite schists, quartzites, marbles) and metamorphosed mafic–ultramafic rocks (amphibolites, talc–tremolite schists, serpentinites; Worku and Schandelmeier 1996; Yihunie 2002; Yibas et al. 2003). In contrast to the Megado belt, the Kenticha OFTB is characterized by a dominance of ultramafic over mafic rocks. The Adola GGC is composed of amphibolite facies quartzo-feldspathic gneisses and biotite-hornblende gneisses as well as deformed metagranitoids. Metamorphic conditions reached 600–650°C and 6–7 kb in the Adola GGC (Yihunie et al. 2004; Tsige 2006) and 520–580°C and 4–5 kb in the Kenticha OFTB (Yihunie et al. 2004).

Deformation and metamorphism of the lithotectonic units of the Adola Belt likely occurred in a collisional setting (Worku and Schandelmeier 1996; Yihunie 2002). East-directed thrusting of the ophiolite associations was followed by right-lateral strike slip movements along these thrust shear zones between 610 and 554 Ma (Yihunie 2002). The granite–gneiss complex and the ophiolitic associations are intruded by postorogenic biotite granite plutons that cut across some of the thrust shear zones (Fig. 2b). Two of these plutons yield U–Pb zircon ages of 554±23 (Robelie granite; Genzebu et al. 1994) and 550±18 Ma (Lega Dima granite; Worku 1996). These ages mark the end of compressive deformation in the Adola Belt and the beginning of postorogenic crustal extension and uplift.

The Kenticha pegmatite field

Although granitic pegmatites can be found in all lithotectonic units of the Adola Belt (Poletayev et al. 1991), a distinct cluster occurs in the Kenticha OFTB southeast of Shakisso (Fig. 2b). These pegmatites are referred to as the Kenticha pegmatite field, which encompasses an area of roughly 2,500 km^2. The pegmatites were emplaced close to, but mainly west of, the NNE–SSW striking Kenticha thrust shear zone (Fig. 3). They intrude greenschist to lower amphibolite facies talc–tremolite schists, chromite-bearing serpentinites, and pelitic to graphitic mica schists. Most of the pegmatites of the Kenticha field strike N–S to NNE–SSW (Fig. 3) but display considerable differences in size (from a few tens of meters to more than 1 km in length), shape (steeply dipping dykes to almost flat lying sheets), internal zoning, mineralogy, and geochemistry (Poletayev et al. 1991). Zerihun (1991) and Zerihun et al. (1995) used mineral parageneses and trace element geochemistry of muscovite and microcline to classify pegmatites of the Kenticha field into barren feldspar–muscovite pegmatites and different types of rare-element pegmatites. Following

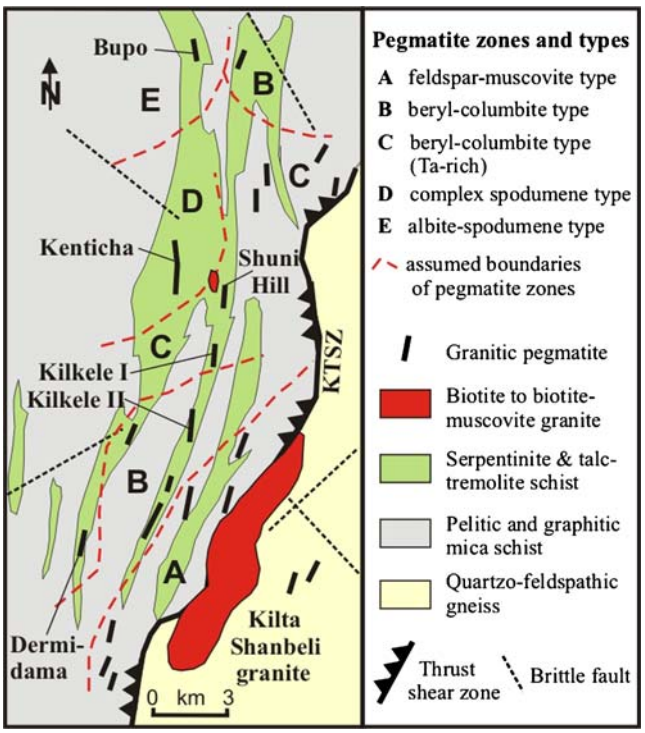

Fig. 3 Regional zoning of the Kenticha pegmatite field (modified after Zerihun et al. 1995)

the paragenetic–geochemical scheme of Černý (1991), the latter pegmatites include representatives of the beryl-type (beryl-columbite subtype), complex-type (spodumene subtype), and albite-spodumene type. All rare-element pegmatites of the Kenticha field belong to the REL-Li subclass based on the updated classification scheme of Černý and Ercit (2005).

Spatial distribution of the different pegmatite types shows a regional zoning pattern relating to the Kilta Shanbeli biotite to biotite–muscovite granite. This elongated pluton is located in the southeastern part of the Kenticha pegmatite field and was emplaced directly east of the Kenticha thrust shear zone (Fig. 3). Pegmatites mainly outcrop to the west and north of the granite, displaying a progressive mineralogical and geochemical differentiation with increasing distance from the Kilta Shanbeli pluton (Zerihun et al. 1995). Earlier investigations (Zerihun 1991; Zerihun et al. 1995; Tadesse and Zerihun 1996) indicated that magmatic fractionation played a fundamental role in the development of the compositional variability and regional zoning of the Kenticha pegmatite field. Stressing the continuity of individual pegmatite dikes and the regular pattern of the regional zoning, Zerihun et al. (1995) suggested a common source for the pegmatites of the Kenticha field. This source is most probably the Kilta Shanbeli biotite to biotite–muscovite granite pluton or related intrusions not exposed at the present surface. The regional zoning starts with barren feldspar–muscovite pegmatites (zone A in Fig. 3) close to the granite pluton. These pegmatites are succeeded by quartz–feldspar–muscovite pegmatites of the beryl-columbite subtype (zone B in Fig. 3), containing black tourmaline, greenish and bluish beryl (aquamarine), and Fe-columbite (Zerihun et al. 1995). The following zone C (Fig. 3) comprises variably zoned and partly albitized quartz–feldspar–muscovite pegmatites of the beryl-columbite subtype. These pegmatites show a higher degree of geochemical differentiation than zone B pegmatites (Zerihun et al. 1995) and contain Mn-tantalite (Tadesse and Zerihun 1996) at Kilkele I and Dermidama (see Fig. 3). Zone D contains a large spodumene-bearing quartz–feldspar–muscovite pegmatite with complex internal zonation and occurrence of Mn-tantalite in its upper part (Tadesse and Zerihun 1996). This pegmatite, known as the main Kenticha pegmatite, is the site of the open pit tantalum mining operations and the main subject of this paper. It is described in further detail below. The final zone E (Zerihun et al. 1995) is located farthest away from the Kilta Shanbeli granite and comprises another highly differentiated spodumene- and Mn-tantalite-bearing pegmatite, known as the Bupo pegmatite (see Fig. 3). This lenticular deeply weathered body is smaller than the Kenticha pegmatite. Due to poor exposure, its internal structure is not known. Since complex zonation has not been observed in this body, the Bupo pegmatite has been provisionally classified as an albite-spodumene type (Zerihun et al. 1995; Tadesse and Zerihun 1996).

Kenticha pegmatite

Size and shape

The Kenticha rare-element pegmatite outcrops on the western flank of a N–S elongated ridge of serpentinite and talc–tremolite schist (Fig. 4a). It is exposed over more than 2 km length and 400–700 m width (Fig. 5). From surface exposure, the Kenticha pegmatite appears as a N- to NNE-striking dyke-like intrusion. The pegmatite pinches out to the south. Its northern termination is concealed under thick alluvium (Poletayev et al. 1991). Exploration and drilling (Poletayev et al. 1991; Zerihun, unpublished data) have demonstrated that the Kenticha pegmatite constitutes a flat-lying to moderately E- to SE-dipping sheet-like intrusion. A generalized roughly E–W oriented cross section is presented in Fig. 6.

The thickness of the pegmatite sheet is highly variable. In locations where both foot wall and hanging wall contacts are exposed, thickness ranges between 40 and 100 m. In the northeastern part of the Kenticha pegmatite, smaller pegmatite veins or apophyses are emanating upwards from the roof of the main intrusion into the country rock (Figs. 5 and 6). Drilling results as well as trenching on the foot slope of the serpentinite ridge to the west of Kenticha pegmatite outcrops have indicated that a separate pegmatite body occurs below the Kenticha pegmatite (Fig. 6; Poletayev et al. 1991).

The Kenticha pegmatite is discordantly emplaced into steeply dipping talc–tremolite and biotite schists and in massive serpentinite. In the northeastern part of the intrusion, large xenolith blocks (mainly serpentinite), measuring 50–100 m (up to maximum 250–500 m) in length and a few meters to 25 m (maximum 50–100 m) in width, occur in the upper part of the pegmatite. These host rock xenoliths are of angular shape and may contain thin pegmatite injections (Poletayev et al. 1991). Alteration reactions with the host rock along the contacts typically resulted in a less than 1-m-thick zone characterized by the development of an exomorphic assemblage described as “glimmerite” by Zerihun (1991; Table 1).

Internal structure and mineral assemblages

The Kenticha pegmatite is internally diversified. It displays an asymmetric textural and mineral zonation (Fig. 6; Table 1). Previous studies (Poletayev et al. 1991; Zerihun 1991; Tadesse and Zerihun 1996) have applied the

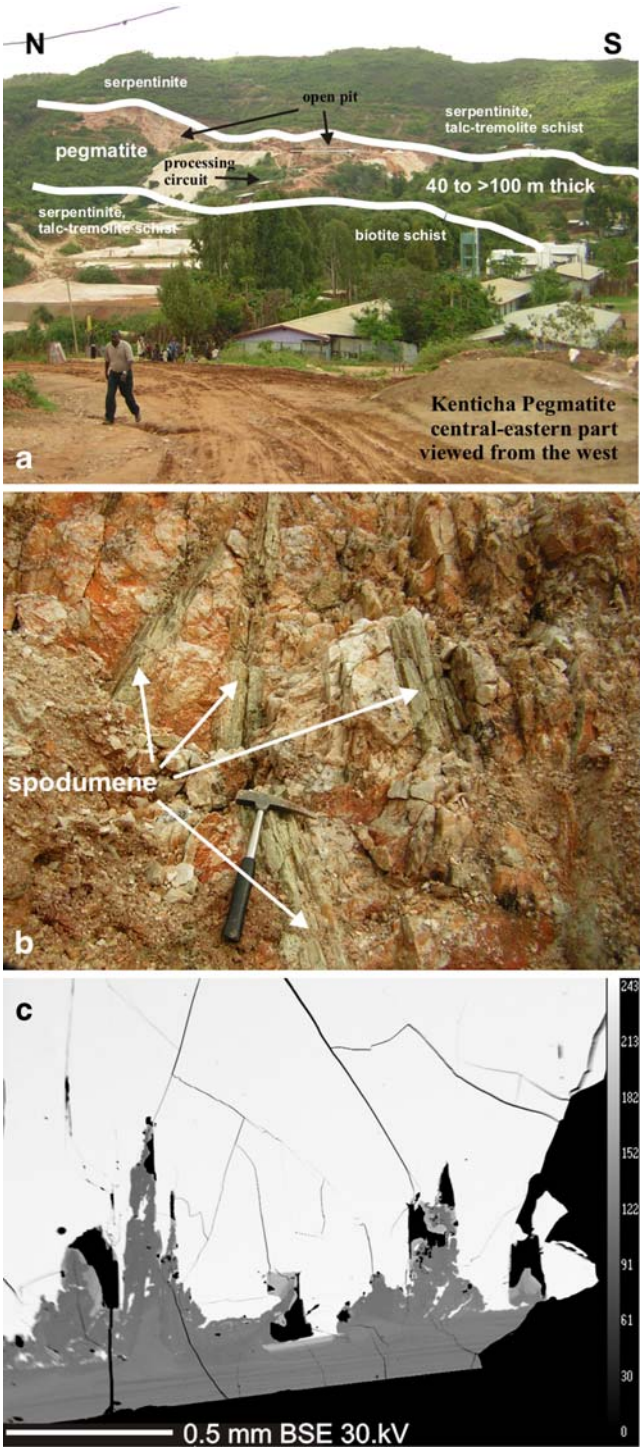

Fig. 4 Photo illustrations showing **a** the south-central part of the Kenticha pegmatite, **b** part of the upper intermediate zone with greenish wedge-shaped spodumene, and **c** BSE image of columbite–tantalite from Kenticha quartz core, showing manganotantalite (*light gray*) replaced along rims and cracks by zoned manganocolumbite (various *shades of dark gray*)

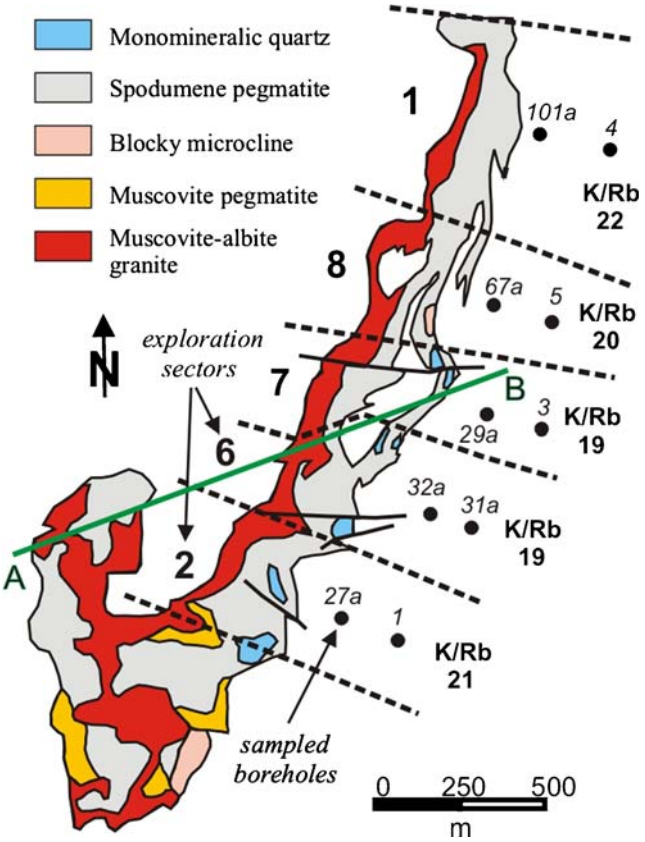

Fig. 5 Simplified geological sketch map of the Kenticha pegmatite (simplified after Poletayev et al. 1991) with location of sampled boreholes. K/Rb ratios are average values of upper zone samples from the two boreholes of each respective exploration sector. *Line A–B* depicts location of schematic cross section in Fig. 6

terminology used for concentrically zoned pegmatites (e.g., Norton 1983) and have outlined seven to nine mineral paragenetic associations or zones, including a border zone, a wall zone, several outer, middle, and inner intermediate zones, as well as a core zone. However, for reasons of simplicity and because of its apparent asymmetry and subhorizontal shape, we have divided the Kenticha pegmatite into three horizontally continuous layers. These internal zones are easiest recognized macroscopically in drill core sections and include a lower zone (LZ), an intermediate zone (IZ), and an upper zone (UZ; Table 1). Thicknesses of the individual zones are, however, highly variable.

The LZ constitutes the basal layer of the Kenticha pegmatite and consists of fine- to medium-grained muscovite–albite granite and aplitic albite–quartz layers with variable proportions of albite, quartz, microcline, and muscovite. The IZ consists of medium- to coarse-grained muscovite–quartz–albite–microcline pegmatite, with tabular to columnar muscovite.

The UZ represents the most voluminous internal zone, making up more than 50% of the whole pegmatite body. It chiefly consists of spodumene-bearing pegmatite (Fig. 4b)

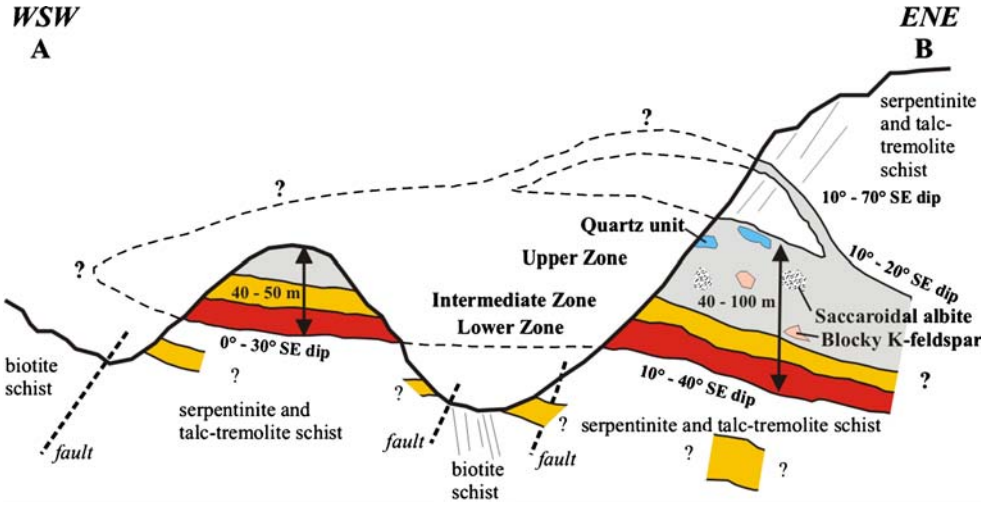

Fig. 6 Schematic cross section (WSW–ENE) of the Kenticha pegmatite. No absolute scale

with discontinuous lenses of blocky microcline, saccharoidal albite, or quartz-rich assemblages. It is thus compositionally differentiated into spodumene, albite, K-feldspar, and quartz units. The *spodumene unit* is effectively continuous (Figs. 5 and 6) and is composed of a coarse-grained muscovite–quartz–albite–microcline–spodumene pegmatite assemblage. Spodumene is greenish-white and characteristically occurs in giant wedge-shaped crystals up to 4 m in length (Fig. 4b), albite displays variable grain sizes, and microcline may be amazonitic in places. The *albite unit* is characterized by high proportion of fine-grained saccharoidal albite and occurs in discontinuous spherical bodies throughout the spodumene-bearing pegmatite. These bodies are rather small in size (<25 m in width) and are locally layered. The *K-feldspar unit* forms discontinuous lenses and consists of giant blocky microcline crystals together with some quartz, muscovite, and minor spodumene. These lenses may reach up to 50 m width, although they are commonly smaller (Poletayev et al. 1991). The *quartz unit* consists of quartz crystals and quartz–lepidolite greisen. It forms discontinuous bodies, measuring 20–100 m in diameter, within the spodumene-bearing pegmatite.

A prominent feature of the Kenticha pegmatite is the almost complete absence of a wall or border zone along the hanging wall contact. Occasionally, a thin pegmatitic

Table 1 Internal structure and mineral assemblages of Kenticha pegmatite, modified after Zerihun (1991), Poletayev et al. (1991), and Tadesse and Zerihun (1996)

	Grain size	Major minerals	Accessory and rare minerals	Ta ore minerals
Exomorphic Zone	Fine grained	Contact assemblage in serpentinite and talc-tremolite schist, 'glimmerite' (phlogopite–quartz–holmquistite–talc–tremolite–actinolite)		
Upper Zone	Coarse grained	Albite–quartz–spodumene–muscovite–microcline–pegmatite, with large spodumene and quartz crystals	Amazonite, apatite, amblygonite, beryl, Li-muscovite, topaz, kunzite, cassiterite, petalite?	Mn-tantalite, ixiolite/wodginite Ta>Nb
discontinuous lenses and spherical bodies	Variable	Monomineralic quartz and quartz-mica assemblages (lepidolite, zinnwaldite)		
	fine grained	Saccharoidal albite		
	coarse grained	Blocky microcline with graphic quartz-feldspar intergrowth		
Intermediate Zone	Medium grained	Muscovite–quartz–albite–microcline pegmatite	Pyrite, ilmenite, magnetite, arsenopyrite	Fe-columbite, Mn-columbite Nb>Ta
Lower Zone	Fine to medium grained	"Alaskitic" muscovite-albite granite to layered albite–quartz aplite	Green tourmaline, garnet, magnetite, pyrite, ilmenite	Columbite Nb>Ta

quartz–microcline–muscovite unit is developed. An exomorphic zone characterized by "glimmerite" is developed at the contact within the ultramafic hanging wall (Table 1). The mineral assemblage of the exomorphic zone includes holmquistite, talc, tremolite, actinolite, phlogopite, and quartz. Late- to postmagmatic alterations of the pegmatite include albitization, amazonitization, sericitization, and greisenization (Zerihun et al. 1995). Kaolinitization is due to deep weathering and is especially prominent in spodumene-rich sections of the pegmatite mined from the open pit.

Major and accessory minerals of the Kenticha pegmatite are listed in Table 1. Accessory minerals include apatite, amblygonite, beryl, lepidolite, topaz, and Mn-tantalite. The compositional range of columbite–tantalite minerals corresponds to pegmatite host units (Table 1). According to Tadesse and Zerihun (1996), Fe- and Mn-columbite is characteristic for granitic LZ and spodumene-free IZ, whereas Ta-rich members (Mn-tantalite) are mainly found in the spodumene-bearing UZ. More details on columbite–tantalite mineralogy and chemistry will be described in a separate section further below.

Mining activity is presently restricted to the upper zone (spodumene and quartz units) in the eastern and northern parts of the Kenticha pegmatite. In the southwestern part of the pegmatite, mineralized parts of the UZ are absent or have been largely eroded (Fig. 6). In contrast to most comparable rare-element pegmatites (e.g., Tanco, Canada, or Greenbushes, Australia), the Kenticha pegmatite rarely carries cassiterite and has no known pollucite.

Sampling and analytical methods

The coarse-grained nature of granitic pegmatites causes problems in determining representative and reliable whole-rock geochemical compositions. Therefore, rare-element pegmatites have mainly been studied geochemically by major and trace element variation in individual minerals or mineral groups (e.g., feldspars, micas, tourmalines, and others). In this study, we used drill core sections, originally taken for grade definition, to characterize the whole-rock geochemistry. We have collected samples from ten exploration boreholes roughly covering the mineralized eastern part of the Kenticha pegmatite along strike and width (Fig. 5). Each sample represents one half of a core section of 5 cm diameter and 1.5 m length.

A total of 84 drill core samples was collected. Samples were assigned to specific pegmatite zones based on drill core logging, i.e., macroscopic identification of texture and mineralogy, petrographic description, borehole depth, and location. Fine- to medium-grained granite- to aplite-textured rocks were assigned to the LZ. Medium- to coarse-grained pegmatitic samples without spodumene were characterized as IZ, while those with spodumene and coarse to giant grain sizes were assigned to the spodumene unit of the UZ. Samples within the UZ with a large proportion of microcline or albite were assigned to the K-feldspar unit and the albite unit, respectively. Samples from the quartz unit were not analyzed due to its nearly monomineralic composition and the resulting very limited geochemical information. In addition, 15 whole-rock samples were collected from granitoid plutons in the near surroundings (Kilta Shanbeli pluton, Shuni Hill pegmatitic granite, Didola plutons) and the Adola Belt (Lega Dima, Adadi Kottan, and Koba Sorsa plutons, see Fig. 2b for location). Whole-rock geochemical analysis of all samples was carried out by X-ray fluorescence (XRF) methods at Technical University of Berlin. Forty-two samples from Kenticha drill core were selected for specific trace element (e.g., Ta, Nb, Be, Li, Y, REE) analysis by inductively coupled plasma mass spectroscopy (ICP-MS) at ACME Labs, Vancouver, Canada.

To complement whole-rock geochemistry, a number of unaltered muscovite samples have been separated from drill core sections of different zones of the Kenticha pegmatite. Additional samples were collected for comparison from surface exposures of the Bupo pegmatite, the Shuni Hill pegmatite, and the Kilkele II pegmatite, representing examples of regional pegmatite zones B, C, and E (Fig. 3). Geochemical analysis of muscovite powders was performed at Bundesanstalt für Geowissenschaften und Rohstoffe (BGR), Hannover. Major and trace elements were analyzed by XRF, except Be, Li, Tl, U, Zn, Hf, and Zr that were analyzed by ICP-MS.

Tantalum–niobium-bearing minerals were collected from surface exposures of the Kenticha, Bupo, and Shuni Hill pegmatites. At Kenticha, samples were also collected from drill core and the ore mineral concentrates. The modal composition of concentrates was analyzed using the mineral liberation analysis (JK Tech Pty Ltd., Australia) on a Quanta 600 FEG scanning electron microscope (FEI company), equipped with an EDAX 32 module. Major and trace elements of Ta–Nb-bearing mineral phases were analyzed by electron microprobe at the BGR (CAMECA SX100) with detection limits of 200 ppm for trace elements. Trace element concentration was also analyzed by different ICP techniques. For conventional solution analysis, hand-picked grains (5 to 100 mg of sample material) were ground and dissolved in a mixture of 48% HF (20–200 μl) and 65% HNO_3 (200 μl). After complete dissolution deionized water was added. Aliquots from this solution were then diluted with 0.15 M HNO_3 and analyzed by ICP-atomic emission spectroscopy (OES) (Nb, Ta, Mn, Fe, Sn) and magnetic sector ICP-MS (32 trace elements including the REE).

For U–Pb dating, Mn-tantalite minerals from the Kenticha (upper zone) and Bupo pegmatites were analyzed. Mineral purification, dissolution, and TIMS analysis were carried out at GFZ Potsdam. Individual Mn-tantalite crystals were crushed. Fragments showing fresh surfaces with a metallic luster were selected under a binocular microscope. The Mn-tantalite fragments were leached in dilute HF using the procedure described in Romer and Smeds (1996) and Baumgartner et al. (2006) and dissolved using 40% HF on a hot plate (160°C), dried, and taken up in 6 N HCl. A ^{205}Pb–^{235}U-mixed tracer and a few microliter H_2SO_4 was added to each sample before dissolution. U and Pb were separated using standard ion-exchange chromatographic procedures. Pb and U were loaded together on single Re-filaments using a silica gel emitter and H_3PO_4 (Gerstenberger and Haase 1997) and measured at 1,200–1,260°C and 1,350–1,400°C, respectively, on a Finnigan MAT262 multicollector mass spectrometer using Faraday collectors and ion counting. Mass fractionation was corrected with 0.1% a.m.u. as determined from the repeated measurement of Pb reference material NBS981.

Whole-rock geochemistry of the Kenticha pegmatite

General geochemical characteristics

Major and trace element geochemical data of the Kenticha pegmatite are listed in Table 2, showing the mean, standard deviation, and range of composition of five individual zones and units. General geochemical characteristics are displayed in Fig. 7a–d. For calculation of the alumina saturation index (ASI), the widely used A/CNK index has been modified to account for the presence of Li-aluminosilicates. The modified A/CNKL index is defined as mol. $Al_2O_3/(CaO + Na_2O + K_2O + Li_2O)$. Rb and Cs have not been incorporated in ASI calculation since contents of their oxides in the Kenticha pegmatite do not significantly effect on the A/CNK(L) value. Li_2O contents have also been included in alkali calculation in the total alkali vs silica (TAS) diagram of Fig. 7a. Values of fractionation indicators (i.e., K/Rb, K/Cs, Nb/Ta, and others) are reported as concentration ratios (gram/gram).

The major element composition of the Kenticha pegmatite and its individual zones is essentially that of a siliceous peraluminous leucogranite. SiO_2 contents (zonal averages) vary from 70–75 wt.%, those of Al_2O_3 from 14.4–16.3 wt.%. CaO, Fe_2O_3, and TiO_2 contents are low in all zones and units (Table 2). MgO contents are also low in the LZ and IZ but are enhanced in the UZ. The major alkali elements show greater variability in the different zones (Table 2; Fig. 7b). Zonal averages vary from 1.1–8.1 wt.% K_2O, 1.8–5.6 wt.% Na_2O, and 0.11–1.64 wt.% Li_2O. There is an even greater variability of the alkali oxides in individual samples of the different zones and units (Table 2; Fig. 7b), which highlights the problem of whole-rock geochemistry in pegmatites due to the very coarse grain size. Average composition of individual zones, however, show distinct geochemical differences and evolutionary trends (discussed below) within the Kenticha pegmatite.

All rocks from the Kenticha pegmatite are peraluminous, but display a generally increasing alumina saturation from LZ to UZ (Table 2; Fig. 7c). This feature is related to increasing spodumene contents and combined higher Al_2O_3 values. The P_2O_5 contents are low and tend to be similar in individual zones (averages vary from 0.13–0.27 wt.%). Such P_2O_5 contents are akin to rare-element granites of the low to intermediate P type (Fig. 7d), considered to be highly fractionated members of I-type granitoids (Linnen and Cuney 2005).

Composition of individual pegmatite zones

The LZ is strikingly sodic with Na_2O contents between 2.63 and 6.99 wt.% and an average of 5.45 wt.%. K_2O contents are low (2.57% on average) but highly variable (0.89–4.67 wt.%). P_2O_5 values are also low (0.13% on average) but have a restricted range (0.07–0.21 wt.%). The granitic rocks of the LZ are peraluminous with an average A/CNKL index of 1.22. They are geochemically specialized, displaying very low Ba (~13 ppm), Sr (~7 ppm), Zr (~25 ppm), ∑REE (<2 ppm), but high Rb (~588 ppm), Cs (~49 ppm), Li (~746 ppm), Be (~168 ppm), Nb (~95 ppm), and Ta (~36 ppm) contents. Values of fractionation indices like K/Rb (36), K/Cs (440), Al/Ga (2,060), Zr/Hf (12), and Nb/Ta (2.6) indicate the highly fractionated nature of the LZ rocks.

The pegmatitic-textured IZ is geochemically very similar to the granitic-textured LZ (Table 2). Compared to the LZ, the IZ has a more potassic composition (Table 2), yet still maintains a sodic character. Although major alkali oxide contents vary widely in individual samples (Table 2; Fig. 7b), values for common fractionation indices are slightly lower than in the LZ (Table 2). Therefore, the IZ appears slightly more geochemically fractionated than the latter (especially in terms of K/Cs ratio).

The UZ is distinguished into three compositional units (the quartz unit as the fourth one has not been analyzed), whose mineralogical characteristics are geochemically reflected in enrichments of K_2O (8.14 wt.%) in the K-feldspar unit, Na_2O (5.62 wt.%) in the albite unit, and Li_2O (1.64 wt.%) in the spodumene unit (cf. Fig. 7c). There is also an increase in peraluminosity from the K-feldspar unit (A/CNKL of 1.24), through the albite unit (A/CNKL of 1.35) to the spodumene unit (A/CNKL of 1.56), which

Table 2 Chemical composition of internal zones and units of the Kenticha pegmatite

	LZ		IZ		UZ K-feldspar Unit		UZ Albite Unit		UZ Spodumene Unit	
	Granite to aplite		Pegmatite		Pegmatite		Pegmatite		Pegmatite	
n	(14; 6 for Li, Be, Ta, Nb)		(13; 7 for Li, Be, Ta, Nb)		(11; 6 for Li, Be, Ta, Nb)		(10; 7 for Li, Be, Ta, Nb)		(35; 19 for Li, Be, Ta, Nb)	
	Mean ± SD	Min–max	Mean ± SD	Min–max	Mean ± SD	Min–max	Mean ± SD	Min–max	Mean ± SD	Min–max
wt. %										
SiO_2	74.7±2.06	70.2–79.2	75.0±2.30	69.3–77.5	70.0±2.20	65.7–74.2	72.6±2.76	68.0–76.4	71.3±4.43	63.8–81.2
Al_2O_3	15.1±1.15	12.1–17.2	14.4±1.55	11.5–16.2	16.3±1.28	13.7–17.8	15.9±1.04	14.1–17.6	16.2±2.35	12.8–21.0
Fe_2O_{3tot}	0.92±0.16	0.54–1.37	0.84±0.32	0.32–1.41	0.73±0.29	0.33–1.14	0.74±0.21	0.38–1.14	1.00±0.33	0.46–1.87
MnO	0.04±0.05	0.01–0.12	0.05±0.06	0.01–0.23	0.02±0.02	0.01–0.08	0.04±0.04	0.01–0.13	0.05±0.04	0.01–0.12
MgO	0.04±0.05	0.01–0.16	0.20±0.16	0.01–0.60	0.71±1.19	0.01–4.02	0.51±0.38	0.01–1.10	1.10±1.21	0.08–5.05
CaO	0.33±0.06	0.23–0.42	0.37±0.13	0.13–0.61	0.26±0.07	0.16–0.35	0.48±0.09	0.36–0.64	0.35±0.26	0.13–1.46
Na_2O	5.45±1.42	2.63–6.99	4.27±2.24	0.95–7.15	1.88±0.68	0.93–3.41	5.62±1.50	3.52–7.96	1.78±1.33	0.16–5.21
K_2O	2.57±1.57	0.89–4.67	3.28±2.99	0.62–8.96	8.14±1.46	6.16–10.07	1.13±0.39	0.87–2.08	2.11±1.39	0.62–5.51
Li_2O	0.16±0.16	0.04–0.48	0.11±0.04	0.05–0.16	0.13±0.05	0.06–0.18	0.34±0.33	0.08–0.99	1.64±0.88	0.41–3.21
TiO_2	0.01±0.01	0.01–0.03	0.01±0.01	0.01–0.02	0.01±0.01	0.01–0.02	0.01±0.01	0.01–0.02	0.01±0.01	0.01–0.02
P_2O_5	0.13±0.04	0.07–0.21	0.18±0.07	0.06–0.32	0.16±0.03	0.12–0.23	0.27±0.07	0.16–0.38	0.16±0.13	0.02–0.71
F	0.04±0.04	0.01–0.12	0.08±0.07	0.01–0.22	0.15±0.09	0.06–0.31	0.07±0.04	0.01–0.14	0.15±0.09	0.04–0.49
LOI	0.67±0.19	0.39–1.00	1.30±0.39	0.87–1.78	1.51±1.13	0.75–3.16	1.41±0.82	0.53–2.42	2.80±1.26	1.25–5.20
Total	99.9±0.60	98.5–100.6	99.3±1.64	97.3–100.9	99.4±1.06	97.9–100.7	99.1±1.70	97.3–101.0	99.61±0.92	97.5–100.5
ppm										
Ba	13±4.2	5–19	19±13	5–50	43±22	5–78	23±12	7–52	34±31	6–188
Sr	7±2.2	3–11	10±5.3	5–25	26±9.6	15–46	24±15	8–55	22±22	5–101
Rb	599±289	178–1,172	918±892	154–3,039	3,122±805	1,933–4,572	462±239	284–975	950±631	262–2,655
Cs	49±27	17–102	100±76	34–260	363±137	190–565	97±50	24–187	201±127	52–732
Ga	39±6.9	27–57	38±6.3	29–52	38±8.7	27–53	45±3.8	40–51	55±9.9	36–71
Be	168±52	86–242	108±46	68–180	31±24	8–65	120±45	64–177	77±57	3–183
Sn	14±10	3–42	16±8.5	1–33	14±9.1	1–34	15±9.6	1–35	30±15	5–76
Nb	95±19	74–117	78±23	41–108	40±21	15–66	125±71	61–270	94±89	20–417
Ta	36±12	19–52	34±12	21–47	42±15	27–67	99±42	51–182	129±135	27–554
Zr	25±8.2	14–40	19±11	8–41	20±24	2–69	19±14	11–56	9.3±4.5	2–27
Hf	2.0±0.5	1.0–2.7	2.2±0.8	1.3–3.5	2.1±1.3	1.1–4.1	2.6±0.7	1.9–3.8	1.6±0.6	0.7–2.5
Zn	185±170	23–666	132±62	30–228	148±98	36–361	153±65	75–305	157±95	51–504
Th	5.3±2.8	1–11	4.5±2.9	1–10	6.2±14.4	1–49	7.0±3.7	3–16	5.6±3.2	1–14
U	4.0±6.2	1–25	2.0±1.6	1–6	1.0±0.01	1–4	4.0±2.3	1–7	1.8±2.3	1–13
K/Rb	36±5.7	28–45	31±5.6	23–40	22±3.6	18–28	22±4.9	15–29	19±3.5	13–28
K/Cs	440±442	105–1,709	243±97	123–452	208±72	113–330	126±93	45–381	96±51	36–202
Al/Ga	2,058±341	1,334–2,764	2,045±383	1,295–2,957	2,368±640	1,708–3,267	1,854±118	1,685–2,058	1,601±261	1,219–2,230
Zr/Hf	12.2±5.4	5.0–22.2	7.8±1.9	5.9–10.9	8.9±5.0	4.7–15.1	8.0±3.8	5.4–14.7	7.2±3.5	4.7–17.5
Nb/Ta	2.6±1.3	1.7–5.3	2.5±0.8	1.6–4.1	1.1±0.7	0.3–1.9	1.3±0.72	0.3–2.3	0.7±0.5	0.3–2.0
A/CNKL	1.22±0.14	1.13–1.50	1.26±0.10	1.16–1.43	1.24±0.09	1.05–1.38	1.35±0.27	1.11–1.91	1.56±0.23	1.04–1.92

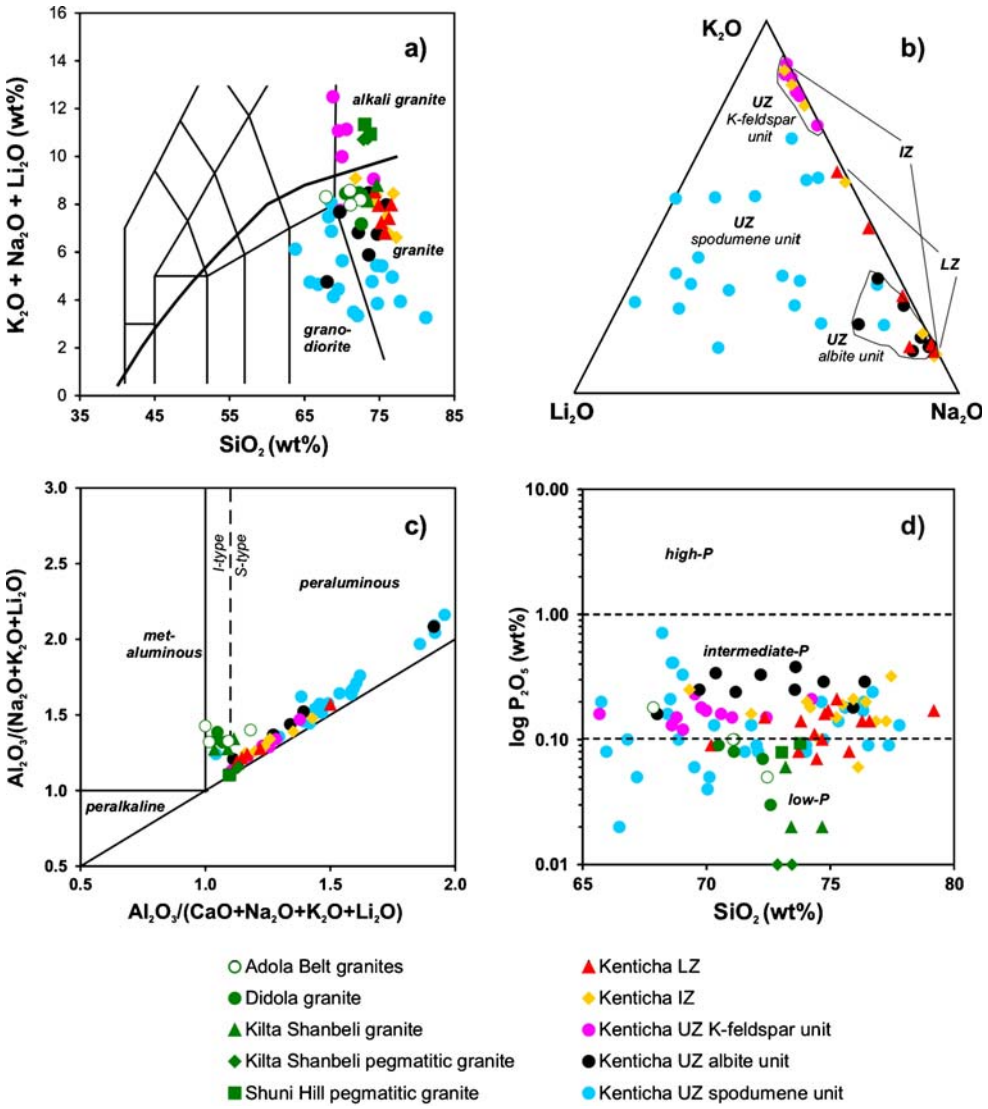

Fig. 7 Major element geochemistry of Kenticha pegmatite and Adola Belt postorogenic granites: **a** total alkalis vs silica diagram, **b** Li_2O–K_2O–Na_2O triplot, **c** ANKL vs ACNKL index (fields for I- and S-type granites from Clarke 1992), and **d** log P_2O_5 vs SiO_2 (based on Linnen and Cuney 2005)

correlates with increasing spodumene and Li_2O contents (0.13 wt.% in the K-feldspar unit, 0.34 wt.% in the albite unit, 1.64 wt.% in the spodumene unit).

The three units of the UZ are similar to the LZ or IZ for major elements, except for SiO_2 in the K-feldspar unit (<70% on average) and Al_2O_3 in both the K-feldspar and spodumene units (>16% on average). P_2O_5 contents are around 0.16 wt.% in both the K-feldspar and spodumene units, i.e., similar to LZ and IZ (Fig. 7d), but slightly enriched (0.27% on average) in the albite unit. Fe_2O_{3tot}, CaO, MnO, TiO_2, Ba, Sr, Th, U, Sn, W, Zr, Hf, Y, and REE all have very low contents in the entire UZ, i.e., in the same range as LZ and IZ.

In the UZ, especially in the spodumene unit, concentrations of MgO are much higher (>1% on average) than in the LZ and IZ. In individual samples, MgO can attain extraordinary values up to 5 wt.% (Table 2). The high MgO contents correlate with the occurrence of secondary carbonate, high loss on ignition (LOI), and strong fracturing of the respective drill core sections. These features probably reflect postmagmatic alteration (possibly veining) in the upper parts of the UZ near the roof of the intrusion. The high MgO content is most likely bound in secondary magnesite and derived from overlying serpentinite and talc–tremolite schists of the hanging wall.

The UZ has the highest contents of incompatible trace elements (Rb, Cs, Ga, Ta) within the Kenticha pegmatite. Pronounced enrichment of Rb (up to 4,570 ppm) and Cs (up to 565 ppm) is encountered in the K-feldspar unit, whereas Ga (up to 71 ppm) and Ta (up to 554 ppm) are the highest in the spodumene unit. The UZ units show very low values for fractionation indices, which, however, vary from one unit to the other (Table 2). Average values of UZ units are K/Rb (22–19), K/Cs (208–96), Al/Ga (2,370–1,700), Zr/Hf (8.9–7.2), and Nb/Ta (1.3–0.7).

Trace element variation and internal differentiation of the Kenticha pegmatite

The lithophile trace elements Rb, Li, Cs, Ga, Ta, Nb, and Be are enriched and display systematic changes within the pegmatite. In contrast, Ba, Sr, and many other trace elements (e.g., Sn, Zr, Hf, REE, Y, Th, U) are remarkably low throughout the pegmatite with no discernible geochemical trends.

Li, Rb, Cs, Ta, and Ga are all progressively enriched from LZ to UZ (Figs. 8a, b and 9), which compares well with the results of studies of other rare-element pegmatites worldwide (Summaries of Černý 1992; Černý et al. 2005). Contents of Be and Nb are highly variable (Nb; Fig. 8c) and Be is depleted overall from LZ to UZ (Fig. 8d). Individual zones and units are transitional and overlap in terms of trace element enrichment (or depletion).

Fractionation indicators (K/Rb, K/Cs, Al/Ga, Nb/Ta, Zr/Hf) reflect different degrees of geochemical evolution with increasing differentiation from the LZ to the UZ-spodumene unit (Table 2; Figs. 8 and 9), the latter one being the most evolved part of the Kenticha pegmatite. Increasing geochemical fractionation toward the interior of pegmatite bodies is a well-known characteristic from other mineralized rare-element granitic pegmatites (Černý 1992, 2005). Variation of fractionation indices in borehole profiles (Fig. 10), however, indicate that fractionation at Kenticha apparently progressed from the bottom to the top of the pegmatite sheet, leading to an asymmetric zonation. A trend of idealized increasing fractionation from the roof to the center of the pegmatite sheet that would reflect a concentric inward solidification process is not documented in the geochemical data (Fig. 10).

Values of fractionation indices and trace element contents are not only controlled by the degree of chemical evolution of the parental melt but also by mineralogical composition of pegmatite zones/units. Such effects can be seen in generally higher values of K/Cs and Al/Ga ratios in

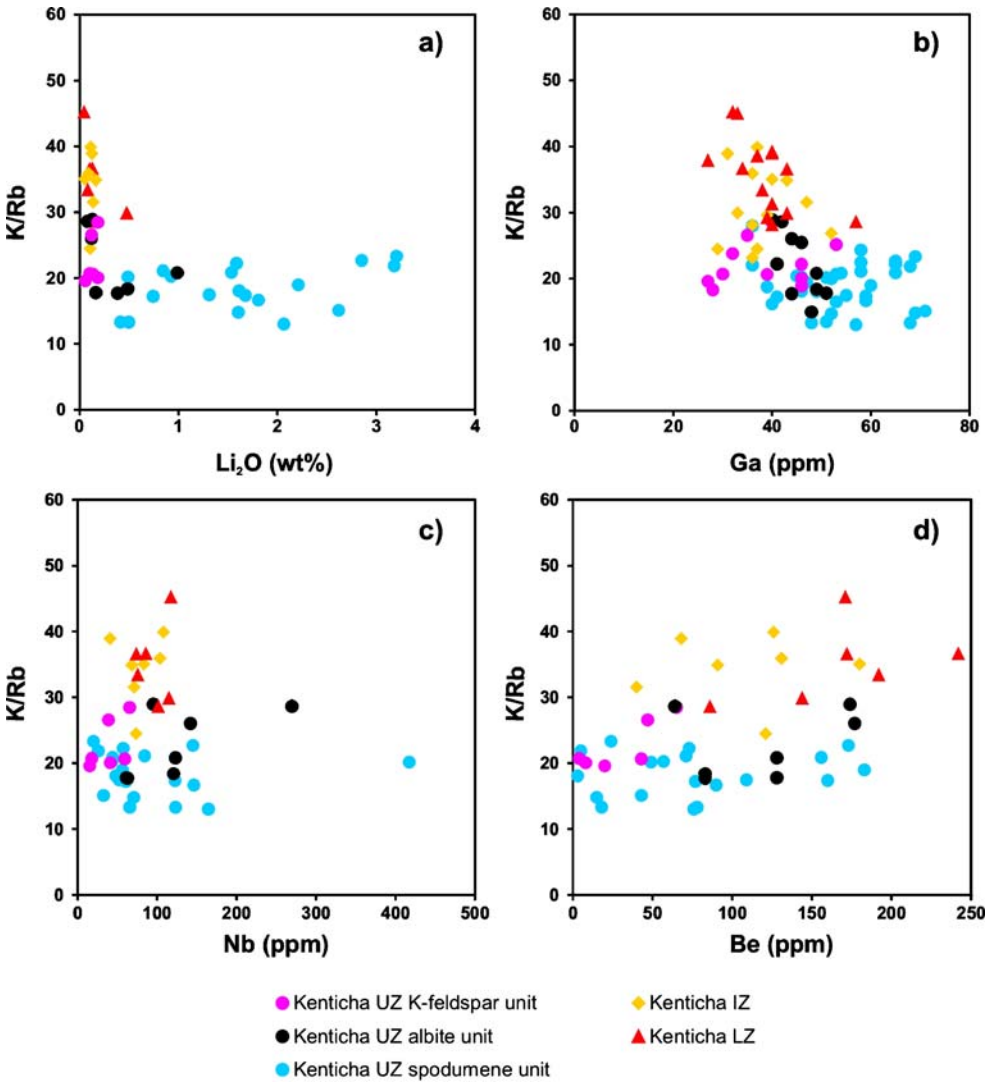

Fig. 8 Trace element variation in whole-rock samples of Kenticha pegmatite: **a** K/Rb vs Li_2O, **b** K/Rb vs Ga, **c** K/Rb vs Nb, and **d** K/Rb vs Be

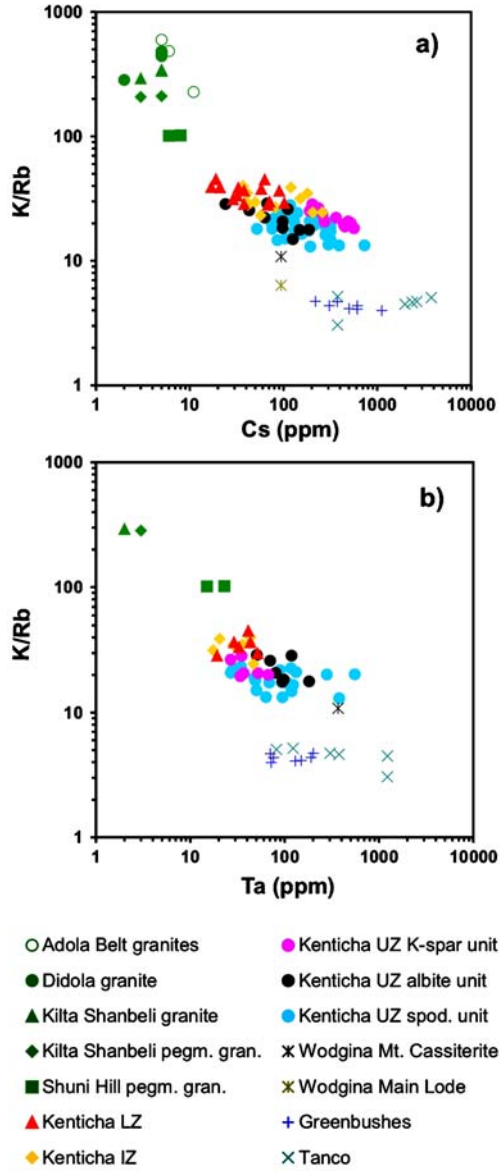

Fig. 9 Bivariate logarithmic plots showing geochemical variation in whole-rock samples from Kenticha pegmatite and Adola Belt postorogenic granites: **a** K/Rb vs Cs and **b** K/Rb vs Ta. Data for Greenbushes, Wodgina, and Tanco pegmatites are from Partington et al. (1995), Sweetapple and Collins (2002), and Stilling et al. (2006)

the K-feldspar unit compared to other units of the UZ (boreholes 3 and 5; Fig. 10), most likely resulting from crystal-chemical differences between microcline, albite, and muscovite (Černý 2005; London 2005a). This mineralogy control on the fractionation indices is much less pronounced for the K/Rb ratio (Fig. 10), which appears to be a more suitable fractionation indicator for whole-rock samples. The Nb/Ta ratio reflects the Ta mineralization potential. It is the lowest in the spodumene unit (as low as 0.3 in individual samples), which is the focus of present mining.

Muscovite chemistry

Average composition of muscovite mica from the Kenticha pegmatite zones and from the Bupo, Shuni Hill, and Kilkele II pegmatites are given in Table 3. The data reveal that the chemical composition of muscovite is relatively constant throughout the different zones of the Kenticha pegmatite as well as in the other three pegmatites. Contents of the three major oxides are slightly variable in individual muscovite samples—SiO_2 (45.4–54.5 wt.%), Al_2O_3 (29.1–36.4 wt.%), K_2O (8.2–10.1 wt.%)—but approach ideal muscovite composition. Low but variable contents of $FeO_{(tot)}$ (0.98–3.17 wt.%) and MgO (0.11–1.20 wt.%) reflect a phengite component in all samples. Na_2O values of 0.38–0.84 wt.% indicate the existence of a minor paragonite component. Li_2O values do not exceed 1.5 wt.% and show that the sampled muscovite from Kenticha does not reach compositions of lithian muscovite or lepidolite.

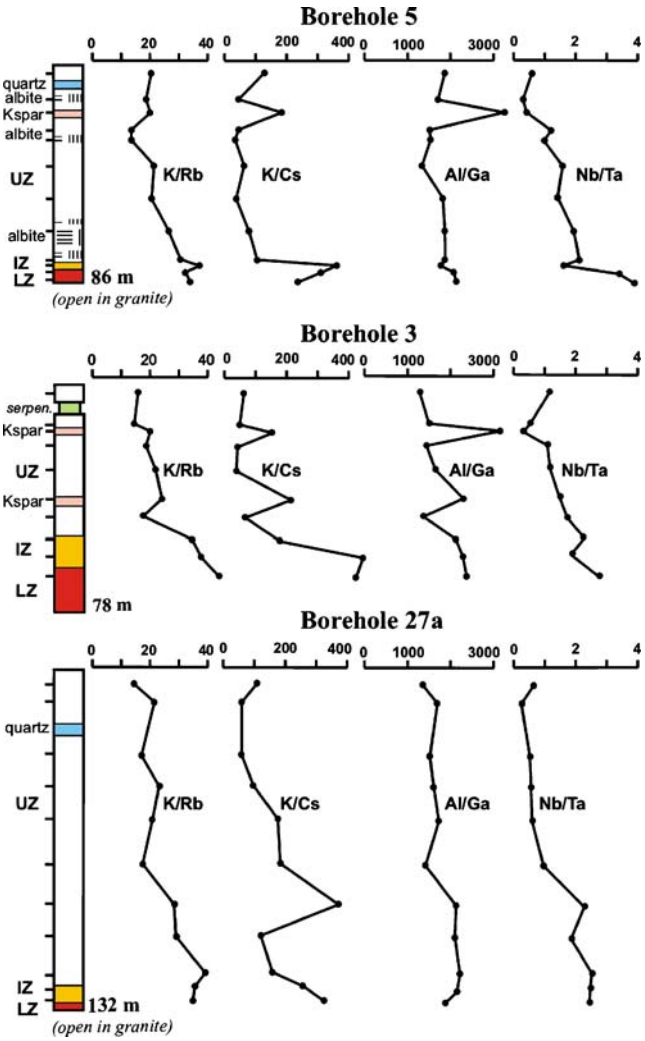

Fig. 10 Variation of fractionation indices in three boreholes compared to macroscopic zoning of the Kenticha pegmatite. For location of boreholes, see Fig. 5

Table 3 Average major and trace element composition of muscovite from Kenticha, Bupo, Shuni Hill, and Kilkele pegmatites

	Kilkele	Shuni	LZ	IZ	Kenticha			Bupo
	II	Hill			UZ albite	UZ Kspar	UZ spod	
n	4	4	2	2	3	5	8	1
wt.%								
SiO_2	46.0	46.7	48.2	48.88	47.0	50.7	48.8	45.4
TiO_2	0.12	0.18	0.09	0.09	0.10	0.07	0.08	0.03
Al_2O_3	33.1	32.6	31.9	31.9	32.4	30.5	32.5	36.4
$FeO_{(tot)}$	3.48	3.06	3.05	2.56	2.96	2.19	2.01	0.96
MnO	0.04	0.08	0.19	0.19	0.22	0.20	0.21	0.24
MgO	0.56	1.25	0.65	0.61	0.77	0.69	0.46	0.05
CaO	0.01	0.01	0.05	0.02	0.03	0.11	0.03	0.03
Na_2O	0.63	0.52	0.63	0.46	0.51	0.60	0.57	0.66
K_2O	9.94	9.92	9.49	9.51	9.79	8.91	9.35	9.59
Li_2O	0.08	0.18	0.54	0.48	1.06	0.92	0.67	0.38
Rb_2O	0.21	0.39	0.36	0.45	0.57	0.63	0.62	1.13
P_2O_5	0.01	0.01	0.02	0.01	0.02	0.08	0.03	0.03
(Cl)	0.01	0.01	0.01	0.01	0.01	0.01	0.01	0.01
(F)	0.05	0.10	0.09	0.10	0.16	0.11	0.09	0.07
LOI	4.83	4.64	4.63	4.75	4.80	4.56	4.65	4.94
Total	99.6	99.6	99.9	100.0	100.4	100.3	100.2	99.9
ppm								
Ba	15	111	7	13	9	14	10	7
Be	11	23	26	37	36	38	29	34
Cs	41	166	135	263	766	793	292	838
Ga	215	233	215	228	239	197	241	283
Hf	0.5	0.5	1.3	0.6	1.0	1.1	0.5	0.3
Nb	497	407	415	322	402	243	258	144
Sn	246	322	242	133	157	115	132	205
Sr	6.3	12	10	11	11	16	14	22
Ta	40	75	67	96	93	84	73	90
Tl	6.2	12	11	14	19	20	21	45
Th	3.8	4.3	6.0	5.0	5.0	9.4	6.9	12
U	0.0	0.0	0.3	0.1	0.4	0.4	0.1	0.0
W	6.5	6.0	35	14	24	11	42	5.0
Zn	198	297	633	568	776	785	790	636
Zr	2.4	2.0	9.3	3.1	5.8	5.0	2.3	1.1
K/Rb	42	22	23	19	16	14	14	7.4
K/Cs	2,896	619	582	330	265	132	294	92
K/Tl	13,453	6,716	6,793	5,345	4,450	3,580	3,734	1,715
Rb/Tl	331	300	294	285	277	260	270	231
Nb/Ta	16	7.5	6.5	4.0	4.7	2.8	3.8	1.6
Fe/Mn	91	48.3	18.7	13.5	13.3	11.1	10.2	4.1
Al/Ga	829	749	788	747	718	761	715	680
Mg/Li	28	13	4.0	5.4	2.2	2.4	3.7	5.6
Zr/Hf	5.3	3.9	6.6	6.1	5.4	4.2	4.6	4.3

Muscovite samples are mineral separates collected from outcrops and drill core sections

In the Kenticha muscovites, the rare alkali elements Rb and Cs show enrichment from LZ to UZ (Fig. 11a, b). Li largely follows this trend (not shown). Within the UZ, Li contents of muscovite from the spodumene unit, however, are lower than in muscovite from the albite and K-feldspar units (see Table 3 for average data), which likely is caused by cogenetic formation of spodumene in the former unit. Li concentration in muscovite from the spodumene-bearing Bupo pegmatite is also low (0.38 wt.% Li_2O). Muscovite from the different UZ units has broadly similar Rb and Cs contents and cannot be ranked in terms of rare alkali concentration. This suggests simultaneous formation of muscovite in all three units over a certain fractionation interval (from K/Tl 5,500 to K/Tl 2,400; Fig. 11b). Muscovite from the K-feldspar and albite units, however, show slightly higher Cs contents at lower (i.e., less

fractionated) K/Rb ratios (Fig. 11a). The rare alkali data in muscovite of the Kenticha pegmatite confirm the trend of increasing fractionation from LZ to UZ, also established from whole-rock data (Fig. 11a). On a regional scale, however, muscovite from the Bupo pegmatite (zone E) is even more fractionated than UZ muscovite from the Kenticha pegmatite (zone D), whereas muscovite from the Shuni Hill pegmatite (zone C) is slightly less or similarly evolved as LZ muscovite from Kenticha (Fig. 11b). Muscovite from the Kilkele II pegmatite (zone B) is the least fractionated (Fig. 11b).

In the Rb/Tl diagram (Fig. 11d), muscovite analyses from the Kenticha, Bupo, Shuni Hill, and Kilkele II pegmatites form a very well-correlated suite. Although the

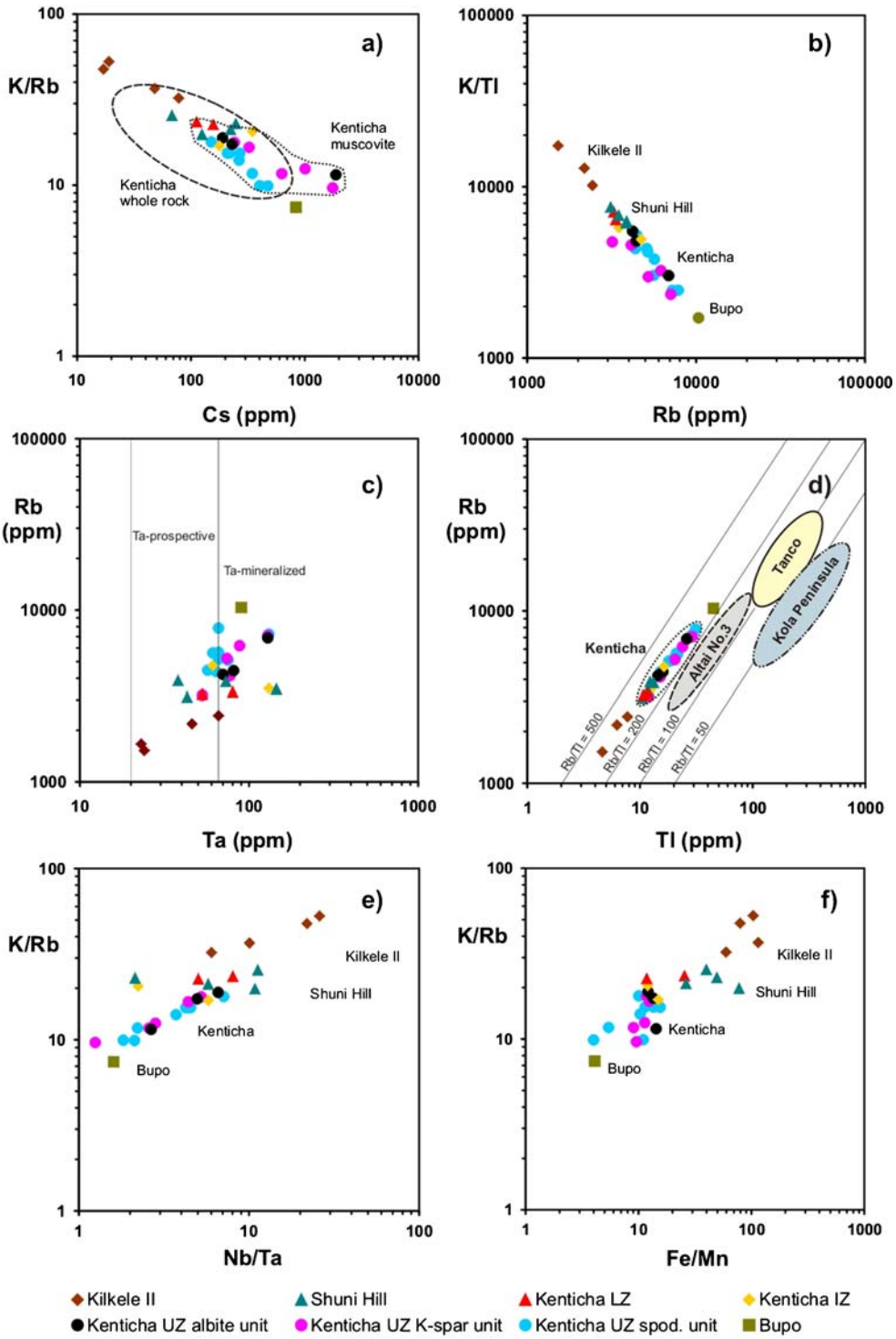

Fig. 11 Bivariate logarithmic diagrams showing chemical variation in muscovite from Kenticha, Bupo, Shuni Hill, and Kilkele II pegmatites: **a** K/Rb vs Cs, **b** K/Tl vs Rb, **c** Rb vs Ta (minimum Ta contents for Ta-prospective and Ta-mineralized pegmatites are from Beus 1966, and Gordiyenko 1971); **d** Rb vs Tl (data for other pegmatite fields are from Černý et al. 1985), **e** K/Rb vs Nb/Ta, and **f** K/Rb vs Fe/Mn

Table 4 Representative electron microprobe analyses of columbite–tantalite, tapiolite, ixiolite, rutile, and cassiterite

Source	Kenticha drill cores												
Mineral	Col(Fe)	Col(Fe)	Col(Fe)	Col(Fe)	Col(Mn)	Col(Mn)	Tan(Mn)	Tan(Mn)	Tan(Mn)	Ixiolite?	Tapiolite	Cassiterite	Rutile(Ta)
Pegmatite zone	LZ	LZ	LZ	IZ	UZ	UZ	UZ	UZ	UZ	UZ	UZ	UZ	UZ
Grains (*n*)	2	3	3	1	2	5	4	1	5	1	2	1	2
Analyses (*n*)	39	6	7	34	24	7	31	2	8	1	4	2	3
Texture	Homogeneous	Core	Rim	Core	Core	Homogeneous	Core	Core	Rim on Col(Mn)	Tan(Mn) intergr.	Homogeneous	Zoned grain	Near cassiterite
SiO_2	bdl	bdl	bdl	bdl	bdl	bdl	bdl	bdl	bdl	bdl	bdl	bdl	2.38
CaO	bdl	bdl	bdl	bdl	bdl	bdl	0.05	bdl	bdl	bdl	bdl	bdl	bdl
Sc_2O_3	bdl	bdl	bdl	bdl	bdl	bdl	bdl	bdl	bdl	bdl	bdl	bdl	bdl
TiO_2	0.91	0.81	0.79	0.26	0.26	0.92	0.11	0.30	0.51	4.17	0.54	0.85	82.00
MnO	8.34	8.07	7.25	8.82	14.03	12.27	11.42	9.74	10.30	7.10	0.70	0.11	0.14
FeO	12.52	12.42	12.30	11.23	5.34	7.27	4.64	6.78	5.60	6.69	14.29	0.90	2.79
ZrO_2	0.15	0.08	bdl	bdl	0.05	0.17	bdl	bdl	bdl	1.08	bdl	bdl	bdl
Nb_2O_5	65.41	63.66	51.82	57.82	55.43	52.47	24.11	23.84	14.78	4.37	0.96	bdl	bdl
SnO_2	bdl	bdl	0.031	bdl	0.035	0.081	bdl	bdl	0.113	5.657	0.222	95.692	1.076
HfO_2	bdl	bdl	bdl	bdl	bdl	bdl	bdl	bdl	bdl	0.607	bdl	0.079	bdl
Ta_2O_5	12.37	14.58	27.03	20.54	24.06	26.39	56.87	57.97	69.39	70.46	81.53	4.49	9.64
WO_3	0.461	0.277	0.390	0.170	0.079	0.235	0.059	0.090	0.061	0.086	0.048	bdl	0.233
UO_2	0.042	bdl	bdl	bdl	bdl	0.225	bdl	bdl	bdl	bdl	bdl	bdl	bdl
PbO_2	na	na	na	na	na	na	na	na	na	na	na	na	na
Total	100.19	99.89	99.62	98.84	99.29	100.03	97.73	98.72	100.80	100.22	98.29	102.12	98.25
Mn*	0.403	0.397	0.374	0.443	0.727	0.631	0.714	0.593	0.651	0.518	0.047		
Ta*	0.102	0.121	0.239	0.176	0.207	0.232	0.587	0.594	0.738	0.907	0.981		

Detection limits for all analyses except UZ/spd tantalite are SiO_2 0.08%, CaO 0.03%, Sc_2O_3 0.03%, ZrO_2 0.03%, Nb_2O_5 0.13%, SnO_2 0.03%, HfO_2 0.02%, WO_3 0.04%, and UO_2 0.03%; detection limits for UZ/spd tantalite are SiO_2 0.05%, CaO 0.03%, ZrO_2 0.08%, SnO_2 0.05%, HfO_2 0.01%, WO_3 0.18%, UO_2 0.00_8%, and PbO2 0.0_2%

Col columbite, *Tan* tantalite, *LZ* lower zone, *IZ* intermediate zone, *UZ* upper zone, *qz* quartz unit, *spd* spodumene unit, *bdl* below detection limit, *na* not analyzed

Rb/Tl ratio shifts from around 350 in the least evolved Kilkele II muscovite to 230 in the Bupo muscovite (Fig. 11d) due to increasing fractionation, the high Rb–Tl correlation infers a cogenetic formation of all four pegmatites from a common magma source. The Rb/Tl ratios of the Kenticha–Bupo–Shuni Hill–Kilkele II pegmatite suite is distinct from other rare-element pegmatite fields (e.g., Tanco, Altai/Keketuohai No.3, or Kola Peninsula; Fig. 11d).

Other trace elements and minor constituents also show fractionation-related depletion and enrichment features in the muscovites from the four pegmatite occurrences. FeO becomes depleted while MnO is enriched with increasing fractionation. Zn is also enriched (Table 3). Among the HFS elements, TiO_2, Sn, and Nb become depleted, whereas Ta is enriched. The relationship of these depletion or enrichment trends with rare alkali fractionation indices (K/Rb, K/Cs or K/Tl) is rather crude, either due to a more complex substitution of these elements for octahedral Al in the muscovite structure or due to occurrence of randomly disseminated micro-inclusions of high-field-strength element (HFSE) oxides (cassiterite, columbite–tantalite) in the muscovite crystals. However, ratio/ratio plots (Fig. 11e, f) clearly show the overall correlation of rare alkali fractionation indices with Nb/Ta and Fe/Mn ratios. The Nb/Ta ratios in Kenticha muscovite are slightly higher (1.2–8.0) than in whole-rock samples (0.3–5) from Kenticha drill core.

Ta contents in muscovite from the four pegmatite occurrences are all above the critical value of 20 ppm used in exploration to identify Ta-prospective pegmatites (Fig. 11c). Muscovite from Kenticha typically falls close to or above the limit of 65–70 ppm used to indicate Ta mineralization. Other trace elements like Be, Ga, or W behave erratically in muscovite. Although there is a general trend of enrichment of these elements (Table 3), positive correlations with fractionation indices (i.e., K/Rb, K/Cs, K/Tl) are very vague.

Chemistry of tantalum–niobium-bearing minerals

Tadesse and Zerihun (1996) characterized the chemical variation of minerals of the columbite–tantalite group in several pegmatites of the Kenticha pegmatite field. In this chapter, we present new data on the mineralogy and mineral chemistry, including trace element data, of Ta–Nb-bearing minerals in the Kenticha, Bupo, and Shuni Hill pegmatites.

Kenticha open pit				Kenticha plant concentrate					Shuni Hill		Bupo		
Tan(Mn) UZ/qz	Col(Mn) UZ/qz	Tan(Mn) UZ/spd	Tan(Mn) UZ/spd	Col(Fe)	Col(Mn)	Col(Mn)	Tan(Mn)	Tan(Mn)	Col(Fe)	Col(Fe)	Col(Mn)	Tan(Mn)	Tan(Mn)
1	1	1	1	23	69	9	15	1	1	33	2	3	1
12	15	15	59	36	92	16	24	1	3	101	61	112	4
Core	Rim	Core	Core						Homogeneous	Homogeneous	Homogeneous	Homogeneous	Homogeneous
bdl	bdl	bdl	bdl	bdl	bdl	bdl	bdl	bdl	bdl	bdl	bdl	bdl	bdl
bdl	bdl	bdl	bdl	bdl	bdl	bdl	bdl	bdl	bdl	bdl	bdl	bdl	bdl
bdl	bdl	na	na	bdl	bdl	bdl	bdl	bdl	bdl	bdl	bdl	bdl	bdl
0.20	0.40	0.06	0.11	1.22	0.67	0.32	0.21	0.14	0.68	0.56	0.35	0.40	0.35
13.82	12.22	14.73	15.03	9.50	13.79	12.14	14.41	13.12	7.35	7.46	14.68	14.43	14.58
0.78	4.82	0.47	0.47	9.66	5.25	5.28	0.54	0.67	11.64	12.12	2.40	1.42	1.24
0.11	bdl	0.10	bdl	0.32	0.12	bdl	0.11	0.24	0.24	0.18	0.16	0.11	0.10
9.61	32.88	18.02	21.07	46.96	49.02	31.32	13.10	2.81	43.28	48.76	35.99	23.72	19.28
0.061	0.077	bdl	0.058	0.083	0.041	0.075	0.061	0.129	0.078	0.083	0.059	0.054	0.071
0.033	bdl	0.019	0.013	0.026	bdl	bdl	bdl	0.104	0.026	0.030	bdl	bdl	bdl
74.85	49.60	65.28	61.84	31.71	30.53	49.70	70.14	80.86	35.74	30.01	45.48	58.59	63.85
bdl	0.072	bdl	bdl	0.175	0.119	bdl	bdl	bdl	0.040	0.125	0.134	0.058	0.041
bdl	bdl	0.009	0.018	0.172	0.141	bdl	bdl	bdl	0.072	bdl	0.142	0.109	0.071
na	na	0.075	0.092	na	na	na	na	na	na	na	na	na	na
99.46	100.06	98.78	98.69	99.83	99.69	98.83	98.57	98.07	99.16	99.34	99.39	98.90	99.58
0.947	0.720	0.97	0.97	0.499	0.727	0.700	0.964	0.952	0.390	0.384	0.861	0.911	0.923
0.824	0.476	0.69	0.64	0.289	0.273	0.488	0.763	0.945	0.332	0.270	0.432	0.598	0.666

Mineralogy and major element composition

Heavy mineral concentrates from the Kenticha processing plant contain minerals of the columbite–tantalite group, microlite, and uranmicrolite. CGM are mainly manganotantalite (60–89%), followed by manganocolumbite (3–40%) and less commonly ferrocolumbite and ferrotantalite. Tapiolite, wodginite, and cassiterite are notably absent from the concentrates. In drill core from Kenticha, CGM (ferrocolumbite to manganotantalite), secondary pyrochlore-group minerals (pyrochlore, microlite, uranmicrolite with up to 6 wt.% UO_2), and rare tapiolite and ixiolite/wodginite are encountered. Cassiterite was found only in one sample of drill hole 27, close to the hanging wall contact. CGM are notably absent in this sample, although Ta-bearing rutile (up to 10 wt.% Ta_2O_5) occurs. Ta–Nb–Fe–W-bearing rutile was also encountered in the uppermost portions of drill hole 101, associated with manganotantalite and a Sn-bearing phase probably akin to wodginite/ixiolite. In the Bupo and Shuni Hill pegmatites, only CGM were encountered.

Major element compositions were measured by electron microprobe at BGR (Table 4). Results are presented in the Mn* (= atomic Mn/(Mn + Fe)) vs Ta* (= atomic Ta/(Ta + Nb)) diagram (Fig. 12). As a whole, CGM composition from Kenticha (drill cores and outcrop material) comprise a trend from ferrocolumbite to manganotantalite (Fig. 12), in general, coinciding with the data of Tadesse and Zerihun (1996). Within the Kenticha drill holes, Mn* and Ta* numbers in CGM tend to increase from the LZ to the UZ and follow whole-rock fractionation indicators. However, Mn fractionation is not as prominent in drill core samples compared to samples collected from the processing plant and the open pit (Fig. 12). CGM collected from the UZ quartz unit outcropping in the open pit plot in the manganotantalite field. Cores of such crystals are homogeneous and Mn–Ta rich and are overgrown and corroded by a second phase characterized by variable and more Nb- and Fe-rich compositions (Fig. 4c and arrows in Fig. 12). Manganotantalite cores occasionally carry metamict grains of uranmicrolite. CGM from Bupo are also Mn-rich (Mn*> 0.85) at variable Ta* (Fig. 12). These grains are fairly homogeneous, but include alteration products such as microlite and plumbomicrolite (up to 20 μm in size). Notably, the compositions of the manganotantalite from Bupo pegmatite and from Kenticha UZ are more Ta rich than most of the analyses presented by Tadesse and Zerihun (1996). At Shuni Hill, CGM have ferrocolumbite compositions with intermediate Mn* (0.40) and Ta* (0.30) numbers (Fig. 12). They straddle the field of the lower and intermediate zones at Kenticha.

In summary, Kenticha has a general evolution trend indicated by CGM from the LZ toward the IZ and UZ and into the quartz unit (Fig. 12). However, considerable

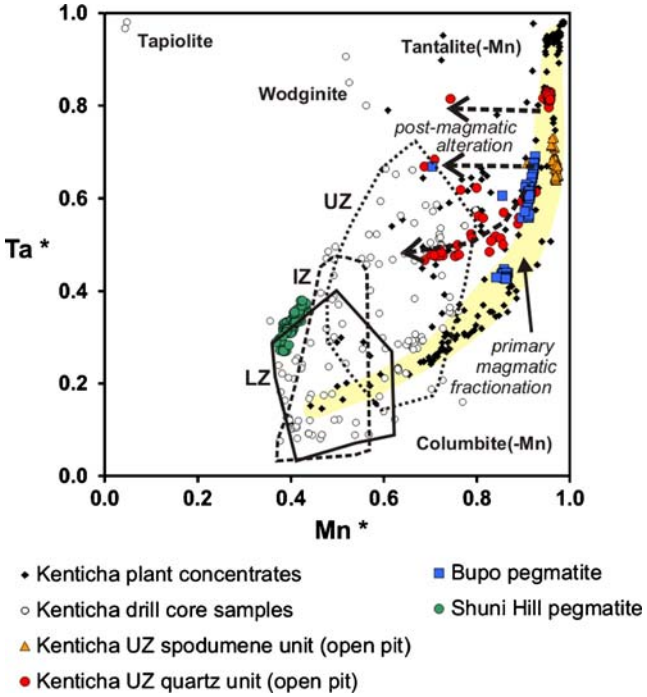

Fig. 12 Variation of Mn* (atomic Mn/Mn + Fe) and Ta* (atomic Ta/Ta + Nb) in CGM from the Kenticha pegmatite field. *UZ* upper zone, *IZ* intermediate zone, *LZ* lower zone. *Arrow* indicates direction of core-rim fractionation within CGM from the UZ quartz unit

differences in characteristic zoning behavior are observed. Whereas some samples from the LZ follow a strong Fe–Mn fractionation trend, Nb–Ta fractionation is more pronounced within the IZ. In the quartz unit and the UZ at Kenticha and at Bupo, Ta–Nb fractionation becomes the most important mechanism. The mechanism producing reversely zoned rims on manganotantalite from the quartz unit and the UZ is as yet unknown. The different degree of Mn–Fe fractionation observed in drill core and outcrop samples may be related to different mineralogical parageneses, e.g., CGM in drill core samples are commonly intergrown with speassartine garnet, whereas those from the pit faces are garnet free.

Trace elements

Minor and trace element concentrations determined by microprobe and ICP-MS reveal considerable variations for some elements (Li, Ti, Sc, Zr, Hf, Sn, W, Th, U, Pb, As, Bi; Table 5). In some crystals, concentrations of U may reach >1,000 ppm. Th varies from 3 to 41 ppm. Sn, Ti, and W decrease with increasing Mn*, whereas Zr increases with Mn*. Sn and Zr are both progressively enriched during Ta–Nb fractionation (increasing Ta*), whereas Ti and W decrease with Ta* (Černý et al. 2007). Zr/Hf ratios range from 0.7 to 7.0, with most samples from Kenticha ranging between 2.0 and 6.2.

Rare earth element concentrations, measured by solution ICP-MS, vary significantly within the studied columbite–tantalite crystals (Table 5; Fig. 13). They show distinctive patterns for each of the three localities. Most manganotantalites from the Kenticha orebody (UZ, quartz unit) are characterized by low total REE and, if any, weak negative Eu anomalies (Fig. 13). Ferrocolumbite, on the other hand, has higher total REE and small though distinct negative Eu anomalies. The REE patterns are generally less fractionated at Kenticha compared to Shuni Hill and Bupo, which both display high La_N/Lu_N ratios. Ferrocolumbite from Shuni Hill has high total REE, strong negative Eu anomalies, and strong MREE/HREE fractionation (Fig. 13). Manganocolumbite and manganotantalite from Bupo both display parallel REE patterns characterized by considerable LREE/HREE fractionation, similar to normal granites, but lack Eu anomalies (Fig. 13).

Mn-tantalite geochronology

U–Pb ages were determined on Mn-tantalite from the UZ spodumene and quartz units of the Kenticha pegmatite and from the Bupo pegmatite (Fig. 3). For geochronology, larger crystals were broken into pieces and fragments with fresh surfaces were selected. The samples were leached in 20% HF and then rinsed in 6 N HCl and 7 N HNO_3 to remove intergrowths and inclusions of silicate and sulfide minerals (cf. Romer and Smeds 1996, 1997) and to selectively dissolve possible metamict sections that might be found around U-rich inclusions (cf. Romer 2003; Smith et al. 2004). The leached Mn-tantalite fragments have relatively low U contents (70–150 ppm; Table 6) and do not show the kind of etching pits characteristic for columbite with much higher and heterogeneously distributed U contents (cf. Romer and Wright 1992; Romer and Smeds 1996). Th contents are low, as indicated by Th/U_{atomic} ratios (Table 6) calculated from the Pb isotopic composition, and the age and U content of the individual samples. Th/U_{atomic} of Mn-tantalite from Kenticha ranges from 0.016 to 0.05 without systematic difference between Mn-tantalite samples from different parts of the Kenticha pegmatite. Mn-tantalite from the Bupo pegmatite has markedly lower Th/U_{atomic} ranging from 0.001 to 0.007 (Table 6). Common (initial) Pb contents ranged from 0.1 to 0.5 ppm Pb (calculated from Table 6), and the isotopic composition of all fragments was highly radiogenic.

Six Mn-tantalite fragments from the quartz unit of the Kenticha pegmatite were analyzed. Five fractions are concordant, whereas one fraction is slightly discordant. All six samples define a discordia with slight excess scatter (MSWD=4.1) that intersects the concordia at 529.2±5.4 Ma (2σ) and passes within error though the

Table 5 Representative bulk analyses of single columbite–tantalite crystals (ICP-MS, ICP-OES)

Locality	Kenticha (plant concentrate)						Kenticha (open pit)		Bupo			Shuni Hill	
Mineral	Col(Fe)	Col(Fe)	Tan(Mn)	Tan(Mn)	Tan(Mn)	Tan(Mn)	Tan(Mn)	Tan(Mn)	Tan(Mn)	Tan(Mn)	Tan(Mn)	Col(Fe)	Col(Fe)
Sample no.	254	254	254	254	250	250	141	141	257	257	257	258	258
at.%													
Mn/(Mn + Fe)	0.44	0.50	0.87	0.94	0.84	0.88	0.94	0.94	0.90	0.90	0.91	0.41	0.39
Ta/(Ta + Nb)	0.28	0.30	0.87	0.94	0.50	0.53	0.85	0.89	0.63	0.71	0.71	0.42	0.45
SnO_2 (wt.%)	0.01	<0.03	0.09	0.03	0.20	0.17	0.03	0.07	<0.03	0.03	0.02	0.04	0.04
ppm													
Sc	72	20	21	6	3	2	2	3	2	3	2	5	4
Ti	5,040	3,710	1,180	555	3,710	2,590	531	739	1,590	1,910	2,120	2,530	2,970
As	<1	<4	<2	<1	<1	<1	<1	<1	<2	<2	<1	<2	<2
Zr	1,420	662	598	313	1,740	1,080	378	1,180	931	1,200	1,340	1,460	1,630
Ba	50	53	37	7	23	12	13	7	28	32	78	36	63
Hf	203	107	819	471	396	245	177	605	253	480	514	281	332
W	3,120	2,390	260	460	1,180	1,110	419	378	489	412	435	1,020	656
Pb	150	344	164	6	182	137	11	24	119	751	357	972	71
Bi	212	133	6	4	86	19	4	4	2	12	5	1	1
Th	21	9	5	3	51	20	3	3	1	8	6	37	10
U	1,230	459	175	28	1,630	910	94	88	946	1,000	1,090	1,040	941
La	1.45	5.68	0.839	0.196	0.697	1.15	0.210	0.200	8.72	25.5	12.3	26.5	9.52
Ce	46.9	12.6	4.04	0.583	11.2	14.8	0.360	0.310	11.5	33.7	13.6	176	14.5
Pr	1.50	2.45	0.091	0.027	0.262	0.561	0.035	0.033	1.97	4.90	2.37	20.3	3.26
Nd	6.91	8.31	0.270	0.078	0.960	1.97	0.115	0.098	6.66	11.0	5.44	81.3	13.0
Sm	4.77	4.36	0.081	0.027	0.132	0.377	0.028	0.084	1.78	2.28	1.13	22.7	11.0
Eu	0.192	0.330	0.018	0.007	0.016	0.035	0.006	0.003	0.329	0.506	0.256	2.00	0.665
Gd	11.1	3.41	0.090	0.028	0.097	0.167	0.056	0.020	1.15	1.54	0.729	29.9	21.7
Tb	5.07	1.03	0.025	0.007	0.011	0.028	0.016	0.007	0.254	0.282	0.141	9.39	6.69
Dy	24.9	4.50	0.162	0.047	0.061	0.175	0.074	0.046	1.47	1.61	0.821	31.0	17.3
Ho	2.13	0.484	0.025	0.007	0.010	0.027	0.009	0.006	0.234	0.265	0.127	1.53	0.838
Er	4.35	1.23	0.079	0.018	0.027	0.072	0.019	0.017	0.604	0.696	0.335	1.70	1.40
Tm	0.792	0.210	0.020	0.005	0.007	0.014	0.003	0.005	0.091	0.107	0.053	0.181	0.194
Yb	6.89	1.70	0.245	0.067	0.060	0.103	0.033	0.042	0.561	0.733	0.359	1.07	1.31
Lu	1.02	0.260	0.079	0.108	0.028	0.036	0.066	0.042	0.110	0.125	0.077	0.163	0.195

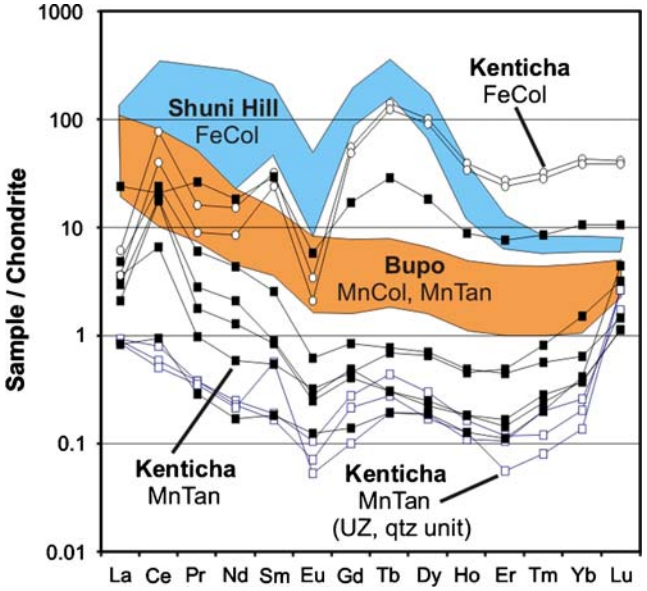

Fig. 13 Ranges of chondrite normalized REE concentrations in columbite–tantalite from Kenticha, Bupo, and Shuni Hill pegmatites. Normalization factors are from McDonough and Sun (2005). Kenticha samples were collected from the processing plant and from the outcropping orebody (UZ quartz unit). *FeCol* ferrocolumbite, *MnCol* manganocolumbite, *MnTan* manganotantalite

concordia diagram origin (Fig. 14a). The five concordant samples define a $^{206}Pb/^{238}U$ age of 530.2±1.3 Ma (2σ), which is considered to be the crystallization age of the Mn-tantalite.

Mn-tantalite from the spodumene unit of the Kenticha pegmatite scatters in the concordia diagram (Fig. 14b) with four samples yielding apparent $^{206}Pb/^{238}U$ ages around 520 Ma and three samples having slightly higher apparent $^{206}Pb/^{238}U$ ages. Two of the samples show a tendency for inverse discordance, i.e., falling above the concordia (Fig. 14b). A discordia based on all seven samples has significant excess scatter, which is removed if the two fractions with reverse discordance are not included in the calculation of the discordia. The remaining samples define a discordia with an upper intercept at 530.0± 2.3 Ma (2σ). This age is interpreted as the crystallization age of the Mn-tantalite.

From the Bupo pegmatite, only four fractions have been analyzed (Table 6). All four fractions are concordant (Fig. 14c) and define an average apparent $^{206}Pb/^{238}U$ age of 530.0±6.4 Ma (2σ) and a concordia age of 529.2± 4.1 Ma (2σ).

The ages from all three Mn-tantalite samples agree within analytical uncertainties. Our data demonstrate that the Kenticha and Bupo pegmatites may have formed coevally and are probably part of the same magmatic system, as had been inferred from their spatial distribution and the systematic variation of mineral content (e.g., Zerihun et al. 1995; Tadesse and Zerihun 1996).

Geochemistry of postorogenic granite plutons

The geochemistry of postorogenic granites was studied on a reconnaissance level to gain an insight into their composition and petrogenetic affiliation (I, S, or A type). Occurrences sampled include the 550±18-Ma Lega Dima pluton (Fig. 2b) and a number of intrusions located in the vicinity of Kenticha (i.e., Koba Sorsa, Adadi Kottan, Didola, Kilta Shanbeli, and Shuni Hill, see Figs. 2 and 3 for location). The postorogenic granites are mainly composed of reddish and gray biotite granite. The Kilta Shanbeli intrusion also contains a muscovite–biotite granite and a K-feldspar-rich pegmatitic granite facies. A similar pegmatitic granite with graphic intergrowth of quartz and K-feldspar crops out in the small Shuni Hills intrusion, located immediately east of the Kenticha pegmatite.

Average geochemical data of the granite samples are presented in Table 7 and graphical display of the data is included in Figs. 7 and 9. All granites are high-K calc-alkaline granites, except the pegmatitic granites from Kilta Shanbeli and Shuni Hill, which have much higher K_2O contents close to 9 wt.% (Table 7) and plot as alkali granite in the TAS diagram (Fig. 7a). All samples are highly siliceous with SiO_2 contents between 70 and 75 wt.% (Fig. 7a). They are mildly peraluminous with A/CNK values between 1–1.1 (Fig. 7c) and have low P_2O_5 content (<0.15 wt.%; Fig. 7d). The overall geochemical characteristics of these granites suggest an I-type affiliation (e.g., Clarke 1992).

Although major element composition of the samples is very similar, trace elements are variable and suggest that the plutons display different degrees of evolution. For example, Rb contents increase from 63 ppm in the least evolved granite (Koba Sorsa granite; Table 7) to 732 ppm in the most fractionated granite (Shuni Hill pegmatitic granite; Table 7). The simultaneous decrease of the compatible elements Sr (from 1,270 to 8) and Ba (from 1,360 to 12; Table 7) indicate that feldspar fractionation played a dominant role in the magmatic differentiation of the granite suite.

Discussion

Internal consolidation and mineralization of the Kenticha pegmatite

The Ta-mineralized Kenticha pegmatite belongs to the spodumene subtype of complex rare-element pegmatites (Černý 1991; Černý and Ercit 2005) and forms a subhorizontal sheet-like intrusion. Whole-rock geochemistry of drill core samples (Table 2), muscovite chemistry (Table 3), and CGM compositional variation (Fig. 12) all demonstrate the highly differentiated nature of the magma from which the Kenticha pegmatite crystallized. K/Rb whole-rock

Table 6 U–Pb analytical data of manganotantalite from Kenticha and Bupo pegmatites

Sample[a]	Weight (mg)	Concentrations (ppm)		^{206}Pb	Th/U (at)	Radiogenic Pb (at.%)[c]				Atomic ratios[c]			Apparent ages (Ma)[d]		
		U	Pb_{tot}	^{204}Pb Measured ratios[b]		^{206}Pb	^{207}Pb	^{208}Pb	$\frac{^{238}U}{^{204}Pb}$	$\frac{^{206}Pb}{^{238}U}$	$\frac{^{207}Pb}{^{235}U}$	$\frac{^{207}Pb}{^{206}Pb}$	$\frac{^{206}Pb}{^{238}U}$	$\frac{^{207}Pb}{^{235}U}$	$\frac{^{207}Pb}{^{206}Pb}$
Kenticha pegmatite (core zone)															
1	0.159	96.3	7.76	2,070	0.023	93.89	5.45	0.66	38,400	0.08624	0.69014	0.05804	533	533	531
2	0.119	70.4	5.67	1,440	0.033	93.63	5.44	0.94	32,500	0.08565	0.68567	0.05806	530	530	532
3	0.103	152	12.3	1,870	0.033	93.60	5.44	0.96	32,800	0.08591	0.68843	0.05812	531	532	534
4	0.071	138	10.5	1,300	0.028	93.76	5.43	0.81	27,200	0.08044	0.64183	0.05787	499	503	525
5	0.248	93.3	7.64	1,200	0.026	93.84	5.42	0.74	16,300	0.08533	0.67993	0.05779	528	527	522
6	0.280	147	12.0	1,770	0.031	93.68	5.43	0.89	23,300	0.08590	0.68607	0.05793	531	530	527
7	0.135	94.1	7.49	1,760	0.022	93.93	5.44	0.63	34,300	0.08496	0.67886	0.05795	526	526	528
Kenticha pegmatite (upper intermediate zone)															
8	0.170	90.8	7.24	1,380	0.022	93.93	5.44	0.63	21,800	0.08403	0.67122	0.05793	520	522	527
9	0.107	87.4	6.92	1,280	0.050	93.18	5.40	1.42	25,200	0.08400	0.67137	0.05797	520	522	528
10	0.533	130	10.2	4,640	0.017	94.08	5.43	0.49	67,650	0.08490	0.67569	0.05772	525	524	519
11	0.336	147	11.7	4,070	0.016	94.11	5.44	0.45	61,800	0.08605	0.68571	0.05779	532	530	522
12	0.162	87.8	7.02	2,410	0.021	93.95	5.45	0.60	54,000	0.08613	0.68898	0.05801	533	532	530
13	0.201	90.5	7.14	1,900	0.030	93.71	5.44	0.85	32,300	0.08392	0.67169	0.05805	520	522	532
14	0.144	178	14.1	1,490	0.017	94.06	5.46	0.49	21,300	0.08371	0.66951	0.05801	518	520	530
Bupo pegmatite															
15	0.161	87.8	7.19	1,190	0.007	94.34	5.46	0.19	17,900	0.08605	0.68698	0.05791	532	531	526
16	0.214	96.4	7.82	1,140	0.004	94.43	5.44	0.13	15,700	0.08477	0.67387	0.05766	525	523	517
17	0.217	107	8.43	2,140	0.001	94.56	5.42	0.02	33,900	0.08451	0.66777	0.05731	523	519	503
18	0.291	94.1	7.69	1,050	0.005	94.41	5.45	0.14	13,700	0.08478	0.67464	0.05771	525	524	519

[a] Fragments for each sample were collected from one single, large Mn-tantalite crystal. Fragments were leached in dilute HF using the procedure described in Romer and Smeds (1996) and Baumgartner et al. (2006) and dissolved using 40% HF on the hot plate (160°C) overnight, dried, and taken up in 6 N HCl overnight. To each sample, a ^{205}Pb–^{235}U-mixed tracer and a few microliter H_2SO_4 were added before dissolution. Pb and U were separated using HBr-HCl and HNO_3-HCl and the ion-exchange chromatographic procedure, respectively. Pb and U were loaded together on single Re-filaments using a silica gel emitter and H_3PO_4 (Gerstenberger and Haase 1997) and measured at 1,200–1,260°C and 1,350–1,400°C, respectively, on a Finnigan MAT262 multicollector mass-spectrometer using Faraday collectors and ion counting

[b] Lead isotope ratios corrected for fractionation (0.1%/a.m.u.)

[c] Lead corrected for fractionation, blank, tracer contribution, and initial lead with $^{206}Pb/^{204}Pb = 17.4 \pm 0.4$, $^{207}Pb/^{204}Pb = 15.48 \pm 0.05$, and $^{208}Pb/^{204}Pb = 37.3 \pm 0.2$. During the measurement period, total blanks were less than 15 pg for lead and less than 1 pg for uranium

[d] Apparent ages were calculated using the constants recommended by IUGS (Steiger and Jäger 1977)

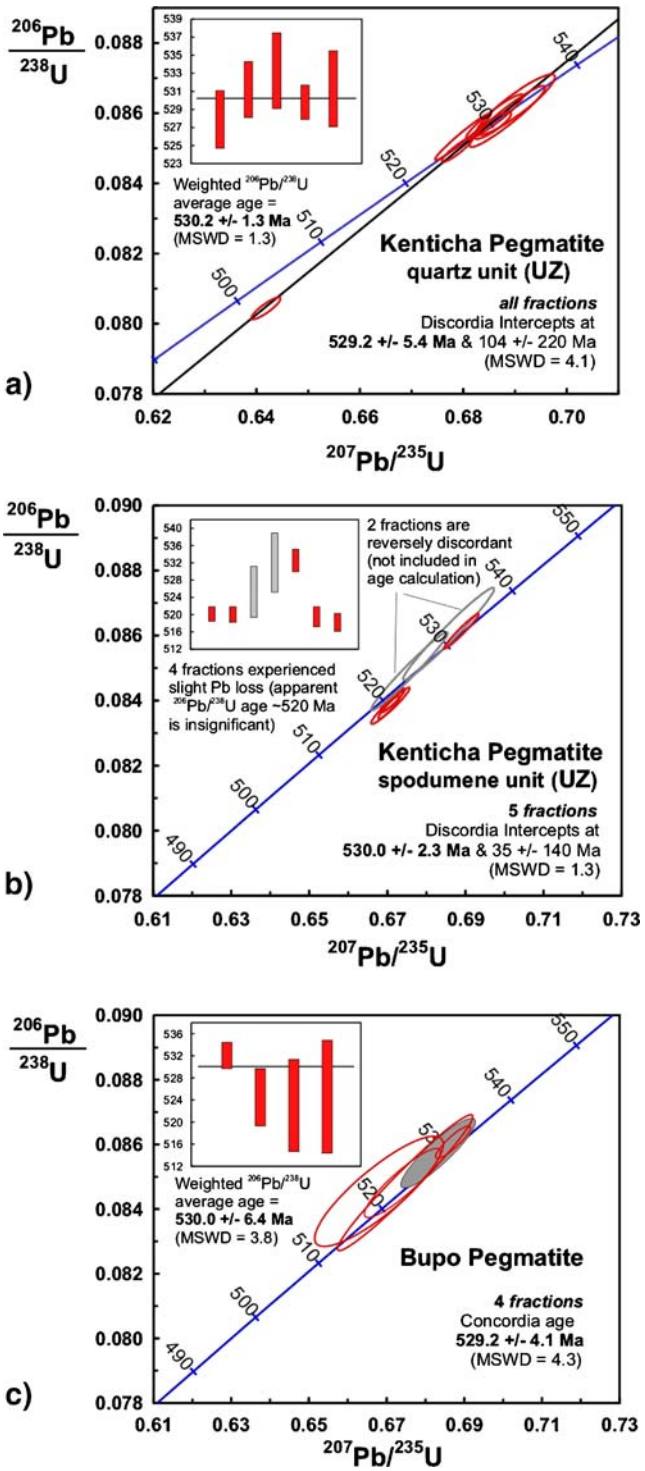

Fig. 14 Concordia diagrams showing the results of Mn-tantalite age determinations: **a** quartz unit (upper zone) of Kenticha pegmatite, **b** spodumene unit (upper zone) of Kenticha pegmatite, and **c** Bupo pegmatite

values vary from a maximum of 45 in the LZ to a minimum of 13 in the UZ; those of muscovite vary from 23.5 (LZ) to 9.5 (UZ). Trace element geochemistry of individual zones and various fractionation indicators in whole rock (K/Rb, K/Cs, Al/Ga, Nb/Ta), muscovite (K/Rb, K/Cs, K/Tl, Rb/Tl, Nb/Ta, Fe/Mn, Al/Ga), and CGM (Mn/Mn + Fe, Ta/Ta + Nb) reveal a geochemical layering, with the least differentiated part of the pegmatite located at the bottom of the intrusive sheet and the most fractionated parts at its top (Figs. 9, 10, 11, and 12). This suggests that crystallization and solidification of the leucogranitic to pegmatitic melt progressed mainly from the bottom (LZ) to the top (UZ).

This upward fractionation of the Kenticha pegmatite has similarities with the internal differentiation of the Tanco pegmatite at Bernic Lake (Canada) that represents a subhorizontal sheet-like intrusion of similar size to Kenticha. At Tanco, consolidation dominantly proceeded from the footwall portion of the pegmatite to the intermediate zones in the upper parts of the intrusion (Černý 2005). However, concentric solidification is evident in the outermost zones, documented by the occurrence of mineralogically and texturally similar lower and upper wall zones (Černý 2005; Stilling et al. 2006). Such incipient forms of downward directed solidification are not observed at Kenticha where an upper wall zone is almost completely lacking or only discontinuously developed. Dominantly, bottom-to-top differentiation has also been observed at the Little Three pegmatite (Morgan and London 1999) and Pinilla de Fermoselle pegmatite (Roda et al. 2005), the latter one constituting the roof zone of a highly differentiated leucogranite intrusion. Both are layered, subhorizontal, but nontantaliferous pegmatites. Bottom-to-top differentiation and asymmetric zonation may thus be a general characteristic of flat-lying sheet-like pegmatite intrusions (London 2008). Complex rare-element pegmatites of different shape and attitude, e.g., the cupola- to plug-like Altai/Keketuohai No.3 pegmatite (Černý et al. 2005; Wang et al. 2007), show clear patterns of concentric inward crystallization.

The geochemical composition of individual zones at Kenticha (Table 2; Figs. 9, 10, 11, and 12) suggest that transitions between them are gradational. Muscovite chemistry from the three mineralogically differentiated UZ units formed at largely similar levels of fractionation (Fig. 11). This may suggest that crystallization occurred rapidly, prohibiting large scale separation of the consolidating crystal mush into distinct continuous layers.

Geochemical variation along strike of the Kenticha pegmatite is insignificant. A spatial comparison of average whole-rock K/Rb ratios from drill core samples of UZ spodumene and albite units reveals that in different parts (i.e., exploration sectors; see Fig. 5) of the Kenticha pegmatite, the UZ displays similar degrees of fractionation (K/Rb~19–22; Fig. 5). The geochemical data shows no variation in degree of fractionation along the strike of the pegmatite, which would follow the interpreted direction of magma injection in the subhorizontal pegmatite sheet. It

thus appears that the magma (± fluid phase) that generated the Kenticha pegmatite was injected in a single pulse and then crystallized essentially in situ without much movement of the consolidating crystal mush. Cooling and solidification proceeded rapidly from the bottom upwards; crystallization occurred probably from significantly undercooled liquids under nonequilibrium conditions (Morgan and London 1999; Webber et al. 1999; London 2005b, 2008). During solidification of the Kenticha pegmatite sheet, heat and volatiles (H_2O, CO_2, F, B) were lost from the consolidating magma into the hanging wall. The emanating volatiles lead to alteration of the ultramafic rocks along the hanging wall contact producing the exomorphic zone ("glimmerite"). Cooling of the melt and high amount of fluids are probably also responsible for the establishment of hydrothermal cells which affected roof parts of the pegmatite sheet and overlying serpentinites and talc–tremolite schists. This is evidenced in high MgO contents, high LOI values, occurrence of secondary carbonates, and increasing fracturing of parts of the UZ. The MgO originates from the ultramafic hanging wall rocks and was introduced into the roof parts of the pegmatite by downward moving, probably carbonaceous fluids. Contamination must have occurred late in the solidification process of the Kenticha pegmatite. Relatively coarse-grained and probably primary magmatic muscovite from the UZ has MgO contents that are comparable or lower than those in less fractionated IZ and LZ muscovite (Table 3). It is thus likely that magmatic crystallization of the Kenticha pegmatite largely occurred under essentially closed system conditions. A similar model has been developed for the Pinilla de Formoselle pegmatite and attributed to rapid, in situ, bottom-up crystallization (Roda et al. 2005, 2006). The Kenticha pegmatite, however, experienced open system behavior during the postmagmatic stage leading to hydrothermal alteration and wallrock contamination.

CGM become increasingly enriched in Ta, Mn, Zr, and Hf from the LZ to the UZ quartz unit of the Kenticha pegmatite (Fig. 12), while REE, Ti, Sc, and other elements become depleted. CGM thus record bottom-to-top fractionation (decreasing Nb/Ta ratios) which corresponds to increasing rare alkali fractionation in whole-rock and muscovite samples (Figs. 9b and 11c, e), indicating that Ta enrichment and tantalite formation is magmatic. Textural attributes of tantalum minerals, i.e., magmatic growth zonation, euhedral grain shape, intergrowth with magmatic phases such as K-feldspar, spodumene, coarse albite, quartz, and spessartine garnet, also support a magmatic origin. Chemical and textural investigations of tantalum oxides in the Lower Tanco pegmatite by Van Lichtervelde et al. (2007) have shown a complex but predominantly magmatic origin of Ta mineralization. Especially the association of columbite–tantalite with microlite and wodginite has been described as primary magmatic (Van Lichtervelde et al. 2007). However, at Kenticha, microlite-group minerals are clearly secondary in origin, replacing Mn-bearing columbite/tantalite.

Ta mineralization at Kenticha is not accompanied by cassiterite. The behavior of Sn appears somewhat unusual, as its concentrations are low in all zones except the quartz unit. Cassiterite becomes stable only in the uppermost levels of the Kenticha pegmatite, coexisting with Ta-bearing rutile instead of columbite–tantalite. Thus, Sn concentrations apparently increase during fractionation and crystallization, but cassiterite saturation was only very locally achieved.

Relationship with surrounding pegmatites and granite plutons

Results of tantalite U–Pb dating indicate that the Kenticha pegmatite and the Bupo pegmatite were both emplaced around 530 Ma (Table 6; Fig. 14). The latter one is situated approximately 9 km to the north of Kenticha (Fig. 3). Coherent Rb/Tl ratios in muscovite from Kenticha, Bupo, Shuni Hill, and Kilkele II pegmatites (Fig. 11d) suggest a cogenetic formation of parts, if not all, of the Kenticha pegmatite field. However, REE patterns in CGM from Kenticha, Bupo, and Shuni Hill are each distinctly different (Fig. 13). These differences may result from (1) formation of CGM in different zones and at different stages of fractionation within the pegmatite(s) (i.e., very low REE in the most fractionated parts), (2) abundance and nature of coexisting REE-incorporating minerals (e.g., garnet, zircon, xenotime, monazite, and others), or (3) different sources of the pegmatite melts. Although REE contents in CGM basically decrease with increasing fractionation of the parental melt, total REE in Bupo CGM are higher than total REE in Kenticha CGM (Fig. 13). However, the former pegmatite is more fractionated (see muscovite chemistry; Fig. 11). Local occurrence of cogenetic minerals which selectively incorporate HREE, such as xenotime, may be responsible for strong MREE/HREE fractionation for example at Shuni Hill. It thus appears that the three studied pegmatites are not related in terms of a strict fractionation sequence Shuni Hill–Kenticha–Bupo. Taking also the coherent muscovite chemistry (Fig. 11) into account, each pegmatite rather represents a separated batch of fractionated melt, with a common source but with individual fractionation histories and local inhomogeneities regarding trace element composition and accessory mineralogy.

The pegmatites of the Kenticha field can temporally be related to the 550–520-Ma postcollisional phase of granitic magmatism in southern Ethiopia (Yibas et al. 2002), although the nearest dated granite plutons (Lega Dima and Robelie; see Fig. 2b) might be slightly older than the Kenticha and Bupo pegmatites. Furthermore, the U–Pb zircon ages of the postorogenic granites are rather imprecise with 554±23 Ma for the Robelie pluton (Genzebu et al.

Table 7 Geochemical composition of postorogenic granites

	Koba Sorsa	Adadi Kottan	Didola	Lega Dima	Kilta Shanbeli	Kilta Shanbeli	Shuni Hill
	Gray bt granite	Reddish bt granite	Gray/red. bt granite	Gray bt granite	2 mica granite	Pegmatitic granite	Pegmatitic granite
n	2	1	4	1	3	2	2
wt.%							
SiO_2	69.5	71.1	71.6	72.5	73.8	73.2	73.4
Al_2O_3	15.6	15.2	15.0	14.0	14.9	14.6	14.7
Fe_2O_{3tot}	2.18	1.82	2.17	2.02	1.14	0.70	0.11
MnO	0.01	0.01	0.02	0.01	0.02	0.01	0.01
MgO	0.56	0.33	0.43	0.16	0.16	0.01	0.03
CaO	1.88	1.36	1.62	1.76	1.27	0.14	0.04
Na_2O	4.07	3.75	4.09	3.04	4.12	1.89	2.18
K_2O	4.08	4.83	4.07	5.15	4.32	8.85	8.96
TiO_2	0.41	0.29	0.26	0.18	0.09	0.03	0.01
P_2O_5	0.14	0.10	0.07	0.05	0.03	0.01	0.09
F	0.06	0.06	0.07	0.06	0.01	0.04	0.05
LOI	0.77	0.75	0.33	0.65	0.40	0.20	0.32
Total	99.4	99.5	99.7	99.5	100.2	99.7	99.9
ppm							
Ba	1,360	896	953	495	294	42	12
Sr	1,270	720	969	149	124	19	8
Rb	63	83	82	188	110	352	733
Cs	6	5	4	11	4	4	7
Ga	18	18	19	18	19	19	24
Li			16		30		
Be			3		3		
Sn	1	1	7	4	2	7	4
Nb	3	3	5	13	6		28
Ta			2		2		19
Zr	163	149	116	131	66	22	5
Hf	5	5	3	5	2		
Y	2	1	12	13	14		3
Th	10	10	8	20	6	13	5
U	3	4	2	5	4	10	3
W	6	1	5	2	6	7	5
Zn	38	41	48	30	13	1	2
K/Rb	541	483	411	227	325	209	102
K/Cs	6,270	8,020	8,440	3,890	8,970	19,600	10,800
Al/Ga	4,690	4,460	4,090	4,120	4,250	4,190	3,300
Zr/Hf	35	32	36	25	28		
Nb/Ta			2.5		3.2		1.5
A/CNK	1.09	1.09	1.06	1.02	1.08	1.13	1.10

1994) and 550±18 Ma for the Lega Dima pluton (Worku 1996). Thus, until more precise geochronological data are available for the granite plutons, a coeval relationship between postorogenic biotite granites and the rare-element pegmatites remains uncertain. The Kenticha pegmatite, however, is definitively not related to the anorogenic A-type granite magmatism, which is dated between 470 and 450 Ma in southwestern Ethiopia (Asrat and Barbey 2003) and southern Somalia (Lenoir et al. 1994).

The postorogenic plutons are all slightly peraluminous high-K calc-alkaline biotite granites with low P_2O_5 contents (Fig. 7). They show a significant compositional range due to magmatic differentiation (Table 7; Fig. 9a) with K/Rb ratios ranging from 400 to 102. The latter value is from the Shuni Hill pegmatitic granite, located very close to the Kenticha pegmatite (Fig. 3). The muscovite–albite granite from the LZ of the Kenticha pegmatite intrusion has an average K/Rb ratio of 36 (Table 2) and may have been derived by further fractionation from the already highly differentiated Shuni Hill granite.

Emplacement of postorogenic granites and pegmatites postdates compressional shear deformation (>550 Ma; Yihunie 2002) in the Adola Belt. The contacts of the Kenticha pegmatite sheet with the wall rocks are sharp and strongly discordant. The steeply dipping schistosity of the talc–tremolite schists and serpentinites apparently did not

control emplacement of the Kenticha pegmatite. The close spatial relationship of the Kilta Shanbeli granite and the pegmatites of the Kenticha field with the Kenticha thrust shear zone (Fig. 3) suggests that movement or reactivation along this structure was involved in the emplacement of the granite–pegmatite system. It is likely that emplacement of the Kenticha pegmatite occurred under conditions of extensional faulting (<550 Ma). Intrusion of the pegmatite probably resulted from a complex interplay of extension-induced opening of tension gashes, magma/fluid overpressure (Brisbin 1986), and intrusion-induced fracture propagation (Baker 1998).

Comparison with other major Ta-mineralized rare-element pegmatites

The size of the Kenticha pegmatite is comparable to other major rare-element pegmatites of the lithium–cesium–tantalum (LCT) clan (Černý 1991), which together constitute most of the World's present Ta reserves. These major pegmatite deposits include Tanco (Černý 2005; Stilling et al. 2006), Greenbushes (Partington et al. 1995), Wodgina/Mt. Cassiterite (Sweetapple and Collins 2002), Volta Grande/São João del Rei (Lagache and Quéméneur 1997; Quéméneur and Lagache 1999), and Altai No.3 (Lu et al. 1997; Wang et al. 2007). They belong to several paragenetic/mineralogical types of rare-element pegmatites (Černý et al. 2005), i.e., complex petalite type (Tanco), complex spodumene type (Greenbushes, Volta Grande, Altai No.3), and albite–spodumene type (Wodgina/Mt. Cassiterite). The Kenticha pegmatite is a member of the complex spodumene type (Zerihun et al. 1995).

All these pegmatites possess similar major element compositions (cf. Černý et al. 2005); however, concentration of certain trace elements in the pegmatites may differ. Figure 9a includes whole-rock K/Rb values and Cs contents of Tanco, Greenbushes, and Wodgina pegmatites. Compared to Kenticha, these Archean pegmatites show higher degrees of rare alkali fractionation, with K/Rb ratios below 10 and mainly around 5. Kenticha K/Rb ratios reach values below 20 only in the UZ spodumene unit and are always above 13–15 (Fig. 9a; Table 2). This clearly indicates the lower overall degree of geochemical evolution of the Kenticha pegmatite. Similarly, whole-rock Cs contents are lower at Kenticha compared to Greenbushes and especially Tanco (Fig. 9a). The only major pegmatites that, similar to Kenticha, display relatively low Cs contents and relatively high K/Rb ratios are those of the Wodgina field (Fig. 9a). The geochemical database of these pegmatites (Sweetapple and Collins 2002), however, is rather restricted. K/Rb ratios in muscovite from the Paleoproterozoic Volta Grande pegmatites (Lagache and Quéméneur 1997; Quéméneur and Lagache 1999) are between 2.0 and 5.3. Respective values for Kenticha muscovite are 10–20 (Fig. 11a; Table 3), revealing again a lower degree of rare alkali fractionation at Kenticha. Other fractionation indicators like K/Cs and Al/Ga in both whole rock and muscovite show trends similar to K/Rb and confirm the apparent lower overall degree of chemical evolution of the Kenticha pegmatite compared to the Archean and Paleoproterozoic rare-element pegmatites. Low Cs contents appear characteristic for pegmatites derived from I-type plutons (LCT-I pegmatites of Černý and Ercit 2005), as opposed to Cs-rich pegmatites derived from S-type granites (LCT-S pegmatites of Černý and Ercit 2005). An I-type derivation of the Kenticha pegmatite corresponds with its low P_2O_5 contents and its classification as a low-phosphorus (I-type) rare-metal granite (Linnen and Cuney 2005).

Differences in HFSE ratios (e.g., Zr/Hf, Nb/Ta) between the Archean to Paleoproterozoic rare-element pegmatites and the early Paleozoic Kenticha rare-element pegmatite appear less strong. Whole-rock Nb/Ta ratios are Tanco (bulk av.) 0.19 (Stilling et al. 2006), Greenbushes 0.12–1.7 (Partington et al. 1995), Wodgina–Mt. Cassiterite 0.07–12, Wodgina Mainlode 0.1–2.7 (Sweetapple and Collins 2002), and Kenticha 0.3–5.3 (Table 2). Whole-rock Ta contents (Fig. 9b) differ less than the rare alkali contents. Although Ta contents in the Kenticha pegmatite are lower than in Tanco pegmatite, they are similar to those of the Greenbushes pegmatite. Thus, the behavior of lithophile (LILE, Rb, Cs) and strongly incompatible elements (HFSE, especially Ta) is decoupled, which would imply that it is not strictly justified to estimate the Ta potential of pegmatites by the degree of fractionation of rare alkali elements.

The different extent of rare alkali fractionation in individual Ta-mineralized LCT pegmatites is most likely related to the nature and composition of the magma and/or protolith and constitutes a source signature (Černý 1989). The Kenticha pegmatite is hosted in juvenile, geochemically rather primitive crust of the Neoproterozoic Arabian–Nubian Shield. The Archean and Paleoproterozoic rare-element pegmatites discussed above are situated within polycyclic Archean crustal terrain, perhaps with the exception of the Wodgina field, which is the oldest (2,800–2,900 Ma, Sweetapple and Collins 2002) among the Archean Ta-mineralized pegmatites. Figure 11d shows Rb and Tl contents in muscovite from Kenticha and some other rare-element pegmatites. The Kenticha muscovites have the lowest Rb and Tl contents and the highest Rb/Tl ratios, just the opposite to Tanco muscovite. This probably indicates derivation of the Kenticha pegmatite from geochemically primitive and rather undifferentiated sources, i.e., juvenile crust or the mantle. The low Tl contents in Kenticha muscovites might also be caused by a previous sulfide extraction and a removal of Tl from the melt. The

concomitantly relatively low Rb concentration, compared to, for example, muscovite from Tanco, however, suggests source geochemistry as the most important factor. The only other major pegmatite deposit that in part shares the rather unevolved Rb/Tl fractionation is the Altai No.3 pegmatite (Fig. 11d) from the Central Asian Orogenic Belt in northwestern China. Similar to Kenticha, the Altai No.3 pegmatite is situated in a segment of rather juvenile crust (mainly Paleozoic in this case), developed within the framework of an accretionary orogen. Such environments represent promising settings for Ta mineralization associated with voluminous postaccretionary (i.e., postorogenic) granitoid magmatism (Küster 2009). This magmatism may have experienced major contributions from the mantle (Dawei et al. 2003) and is characterized by contemporaneous emplacement of LCT and NYF granite/pegmatite suites (Dawei et al. 2003; Küster 2009). The Altai No.3 pegmatite is of Late Triassic age (220–213 Ma) and apparently formed during anorogenic extension (Wang et al. 2007). Formation of granitoid-hosted LCT-type rare-metal mineralization may thus well extent from the postorogenic into the anorogenic stage.

Conclusions

1. The whole-rock geochemical composition of the Kenticha pegmatite corresponds to a peraluminous highly silicic leucogranite, strongly enriched in lithophile elements, especially Li, Rb, Cs, Ga, and Ta. Low P_2O_5 contents of the pegmatite are akin to rare-metal granitoids of the low- to intermediate-P type.
2. The internal evolution of the subhorizontal pegmatite sheet at Kenticha is primarily characterized by bottom-to-top in situ fractionation, which accounts for the observed chemical and mineralogical zonation within the pegmatite, including tantalite mineralization. Crystallization occurred mainly under closed system conditions. Contamination from the hanging-wall ultramafic rocks occurred only during postmagmatic hydrothermal stages.
3. U–Pb tantalite dating of the Kenticha pegmatite has revealed that emplacement and mineralization occurred at 530 Ma. U–Pb tantalite dating of the nearby Bupo pegmatite yielded the same age, indicating that both pegmatites may be coeval. The trace element chemistry of muscovite from different pegmatites of the Kenticha field suggests a cogenetic formation.
4. The formation of the pegmatites is related to postorogenic granitoid magmatism in the Adola Belt (550–520 Ma). Plutons of this slightly peraluminous I-type granite suite form a geochemically differentiated series in the surroundings of Kenticha. Highly fractionated members of this series are likely parental magmas of the pegmatites.
5. The Kenticha pegmatite is less evolved in terms of rare alkali fractionation than late Archean and Paleoproterozoic Ta-mineralized rare-element pegmatites (e.g., Wodgina, Tanco, Greenbushes, Volta Grande). The overall "moderate" geochemical evolution probably is a source signature, as the Kenticha pegmatite is hosted in juvenile crust. Ta contents and Nb/Ta fractionation of the Kenticha pegmatites, however, are comparable to Archean Ta-pegmatites.

Acknowledgments The authors are grateful to the German Academic Exchange Service (DAAD) for granting a research fellowship to D. Küster at TU Berlin and a visiting scholarship to D. Tolessa at Bundesanstalt für Geowissenschaften und Rohstoffe (BGR) in Hannover. The support of Mekelle University through a field research grant to D. Küster and K. Bheemalingeswara is much appreciated. We acknowledge the logistic support of the Geological Survey of Ethiopia and the Ethiopian Mineral Development Share Company, especially their crews at Kenticha Mine and Shakisso. We thank Dr. G. Matheis (TU Berlin) for his support and cooperation and P. Marsiske (TU Berlin) for XRF analysis. Thanks go also to the following persons at the BGR laboratories for their analytical input: P. Rendschmidt (polished and thin sections), F. Korte (XRF), H. Lorenz (ICP-MS), and J. Lodziak (electron microprobe). Marcus Sweetapple is thanked for his careful review and constructive comments. Finally, we are indebted to the Director of Ethiopian Mineral Development Share Company for his allowance to publish the data.

References

Abraham A, Hassen N, Yemane T, Genzebu W, Seyid G, Mehari K, Alemu T (1992) The geological evolution of the proterozoic of southern Ethiopia. Abstr Vol 29th Intern Geological Congress, Kyoto, Japan, p 13

Asrat A, Barbey P (2003) Petrology, geochronology and Sr–Nd isotopic geochemistry of the Konso pluton, south-western Ethiopia: implications for transition from convergence to extension in the Mozambique Belt. Int J Earth Sci (Geol Rundsch) 92:873–890

Baker DR (1998) The escape of pegmatite dikes from granitic plutons: constraints from new models of viscosity and dike propagation. Can Mineral 36:255–263

Baumgartner R, Romer RL, Moritz R, Sallet R, Chiaradia M (2006) Columbite–tantalite bearing granitic pegmatites from the Seridó Belt, northeastern Brazil: genetic constraints from U–Pb dating and Pb isotopes. Can Mineral 44:69–86

Beraki WH, Bonavia FF, Getachew T, Schmerhold R, Tarekegn T (1989) The Adola Fold and Thrust Belt, southern Ethiopia: a re-examination with implications for Pan-African evolution. Geol Mag 126:647–657

Beus AA (1966) Distribution of tantalum and niobium in muscovites from granitic pegmatites. Geokhimiya 10:1216–1220, in Russian

Brisbin WC (1986) Mechanics of pegmatite intrusion. Am Mineral 71:644–651

Černý P (1989) Contrasting geochemistry of two pegmatite fields in Manitoba: products of juvenile Aphebian crust and polycyclic Archean evolution. Precambr Res 45:215–234

Černý P (1991) Rare-element granitic pegmatites. Part I: anatomy and internal evolution of pegmatite deposits. Geosci Can 18:49–67

Černý P (1992) Geochemical and petrogenetic features of mineralization in rare-element granitic pegmatites in the light of current research. Appl Geochem 7:393–416

Černý P (2005) The tanco rare-element pegmatite deposit, Manitoba: regional context, internal anatomy, and global comparisons. In: Linnen RL, Samson IM (eds) Rare element geochemistry and mineral deposits. Geol. Assoc. Canada (GAC) short course notes 17. Geological Association of Canada, Toronto, ON, pp 127–158

Černý P, Ercit TS (2005) The classification of granitic pegmatites revisited. Can Mineral 43:2005–2026

Černý P, Meintzer RE, Anderson AJ (1985) Extreme fractionation in rare-element granitic pegmatites: selected examples of data and mechanisms. Can Mineral 23:381–421

Černý P, Blevin PL, Cuney M, London D (2005) Granite-related ore deposits. Econ Geol 100:337–370

Černý P, Ercit TS, Smeds S-A, Groat LA, Chapman R (2007) Zirconium and hafnium in minerals of the columbite and wodginite groups from granitic pegmatites. Can Mineral 45:185–202

Clarke DB (1992) Granitoid rocks. Topics in earth sciences 7. Chapman & Hall, London, 283p

Dawei H, Shiguang W, Xilin X, Jisheng Z, Tao W (2003) Metallogenetic province derived from mantle sources: Nd, Sr, S, Pb isotope evidence from the Central Asian Orogenic Belt. Gondwana Res 6:711–728

Emelyanov EL, Abebaw T, Tesfaye T, Teweldemedhin T (1986) Preliminary report on prospecting results of the Kenticha rare metal deposit.—Internal report (unpubl) Ethiopian Mineral Resource Development Corp, Ministry of Mines and Energy, Addis Ababa

Genna A, Nehlig P, Le Goff E, Guerrot C, Shanti M (2002) Proterozoic tectonism of the Arabian Shield. Precambr Res 117:21–40

Genzebu W, Hassen N, Yemane T (1994) Geology of the Agere Mariam area. Ethiopian Institute of Geological Surveys, memoir 8. Ethiopian Institute of Geological Surveys, Addis Ababa, 23p

Gerstenberger H, Haase G (1997) A highly effective emitter substance for mass spectrometric Pb isotope ratio determinations. Chem Geol 136:309–312

Gichile S (1991) Structure, metamorphism and tectonic setting of a gneissic terrane, the Sagan-Aflata area, southern Ethiopia. Unpubl MSc thesis, University of Ottawa, Canada, 225p

Gordiyenko VV (1971) Concentration of Li, Rb and Cs in potash feldspar and muscovite as criteria for assessing the rare metal mineralization in granitic pegmatites. Int Geol Rev 13:134–142

Johnson PR, Woldehaimanot B (2003) Development of the Arabian–Nubian Shield: perspectives on accretion and deformation in the northern East African Orogen and the assembly of Gondwana. In: Yoshida M, Windley BE, Dasgupta S (eds) Proterozoic East Gondwana: supercontinent assembly and breakup. Geological Society of London special publication 206. Geological Society of London, London, pp 289–325

Kozyrev V, Girma K, Bekele WM, Teweldemedhin T (1982) Regional geological and exploration work for gold and other minerals in the Adola gold fields.—Internal report (unpubl) Ethiopian Mineral Resource Development Corp, Ministry of Mines and Energy, Addis Ababa, 260p

Kozyrev V, Girma K, Safonov J, Tuliankin V, Bekele WM, Bestujev A, Darijapov A, Teweldemedhin T, Gurbanivich G, Kaitukov M, Arijapov A (1988) Geological map of the Adola Region, 1:100000. Ethiopian Mapping Agency, Addis Ababa

Küster D (2009) Granitoid-hosted Ta mineralization in the Arabian–Nubian Shield: ore deposit types, tectono-metallogenetic setting and petrogenetic framework. Ore Geol Rev 35:68–86

Lagache M, Quéméneur J (1997) The Volta Grande pegmatites, Minas Gerais, Brazil: an example of rare-element granitic pegmatites exceptionally enriched in lithium and rubidium. Can Mineral 35:153–165

Lenoir JL, Küster D, Liégeois JP, Utke A, Haider A, Matheis G (1994) Origin and regional significance of Late Precambrian and Early Paleozoic granitoids in the Pan-African belt of Somalia. Geol Rundsch 83:624–641

Linnen RL, Cuney M (2005) Granite-related rare-element deposits and experimental constraints on Ta–Nb–W–Sn–Zr–Hf mineralization. In: Linnen RL, Samson IM (eds) Rare element geochemistry and mineral deposits. Geol Assoc Canada (GAC) short course notes 17. Geological Association of Canada, Toronto, On, pp 45–68

London D (2005a) Geochemistry of alkalis and alkaline earths in ore-forming granites, pegmatites, and rhyolites. In: Linnen RL, Samson IM (eds) Rare element geochemistry and mineral deposits. Geol Assoc Canada (GAC) short course notes 17. Geological Association of Canada, Toronto, On, pp 17–43

London D (2005b) Granitic pegmatites: an assessment of current concepts and directions for the future. Lithos 80:281–303

London D (2008) Pegmatites. Can Mineral Spec Publ 10:347

Lu HZ, Wang ZG, Li YS (1997) Magma-fluid transition and the genesis of pegmatite dike No.3, Altay, Xinjiang, northwest China. Chin J Geochem 16:43–52

McDonough WF, Sus S-s (2005) The composition of the earth. Chem Geol 120:223–253

Morgan GBVI, London D (1999) Crystallization of the little three layered pegmatite–aplite dike, Ramona District, California. Contrib Mineral Petrol 136:310–330

Norton JJ (1983) Sequence of mineral assemblages in differentiated granitic pegmatites. Econ Geol 78(854–87):4

Partington GA, McNaughton NJ, Williams IS (1995) A review of the geology, mineralization, and geochronology of the Greenbushes pegmatite, Western Australia. Econ Geol 90:616–635

Poletayev JA, Verbvsky ON, Teweldemedhin T, Musa E, Alemayehu B, Manaye Y (1991) The geology and rare metal potential of the Kenticha pegmatite deposit. Internal report (unpubl) Ethiopian Mineral Resource Development Corp, Ministry of Mines and Energy, Addis Ababa, 113p

Quéméneur J, Lagache M (1999) Comparative study of two pegmatitic fields from Minas Gerais, Brazil, using Rb and Cs contents of micas and feldspars. Rev Brasil Geociências 29:27–32

Roda E, Pesquera A, Gil-Crespo PP, Torres-Ruiz J, Fontan F (2005) Origin and internal evolution of the Li–F–Be–B–P-bearing Pinilla de Fermoselle pegmatite (Central Iberian Zone, Zamora, Spain). Am Mineral 90:1887–1899

Roda E, Pesquera A, Gil-Crespo PP, Torres-Ruiz J, De Parseval P (2006) Mineralogy and geochemistry of micas from the Pinilla de Fermoselle pegmatite (Zamora, Spain). Eur J Mineral 18:369–377

Romer RL (2003) Alpha-recoil in U–Pb geochronology: effective sample size matters. Contrib Mineral Petrol 145:481–491

Romer RL, Smeds SA (1996) U–Pb columbite ages of pegmatites from Sveconorwegian terranes in southwestern Sweden. Precambr Res 76:15–30

Romer RL, Smeds SA (1997) U–Pb columbite chronology of post-kinematic Palaeoproterozoic pegmatites in Sweden. Precambrian Res 82:85–99

Romer RL, Wright JE (1992) U–Pb dating of columbites: a geochronologic tool to date magmatism, metamorphism, and ore deposits. Geochim Cosmochim Acta 56:2137–2142

Smith SR, Foster GL, Romer RL, Tindle AG, Kelley SP, Noble SR, Horstwood M, Breaks FW (2004) U–Pb columbite–tantalite chronology of rare-element pegmatites using TIMS and laser ablation-multi collector-ICP-MS. Contrib Mineral Petrol 147:549–654

Steiger RH, Jäger E (1977) Subcommission on geochronology: convention on the use of decay constants in geo- nad cosmochronology. Earth Planet Sci Letters 36:359–362

Stern RJ (1994) Neoproterozoic (900–550 Ma) arc assembly and continental collision in the East African Orogen: implications for consolidation of Gondwanaland. Ann Rev Earth Planet Sci 22:319–351

Stilling A, Černý P, Vanstone PJ (2006) The Tanco Pegmatite at Bernic Lake, Manitoba. XVI. Zonal and bulk composition and their petrogenetic significance. Can Mineral 44:599–623

Stoeser DB, Camp VE (1985) Pan-African microplate accretion in the Arabian Shield. Geol Soc Am Bull 96:817–826

Sweetapple MT, Collins PLF (2002) Genetic framework for the classification of Archean rare metal pegmatites in the North Pilbara Craton, Western Australia. Econ Geol 97:873–895

Tadesse S, Zerihun D (1996) Composition, fractionation trend and zoning accretion of the columbite–tantalite group of minerals in the Kenticha rare metal field (Adola, southern Ethiopia). J Afr Earth Sci 23:411–431

Teklay M, Kröner A, Mezger K, Oberhänsli R (1998) Geochemistry, Pb–Pb single zircon ages and Nd–Sr isotope composition of Precambrian rocks from southern and eastern Ethiopia: implications for crustal evolution in East Africa. J Afr Earth Sci 26:207–227

Tsige L (2006) Metamorphism and gold mineralization of the Kenticha–Katawicha area, Adola Belt, southern Ethiopia. J Afr Earth Sci 45:16–23

Tsige L, Abdelsalam MG (2005) Neoproterozoic–early Phanerozoic gravitational tectonic collapse in the southern part of the Arabian Shield: the Bulbul Belt of southern Ethiopia. Precambr Res 138:297–318

Van Lichtervelde M, Salvi S, Béziat D, Linnen RL (2007) Textural features and chemical evolution in tantalum oxides: magmatic versus hydrothermal origins for Ta mineralization in the Tanco Lower pegmatite, Manitoba, Canada. Econ Geol 102:257–274

Wang T, Tong Y, Jahn BM, Zou TR, Wang YB, Hong DW, Han BF (2007) SHRIMP U–Pb zircon geochronology of the Altai No. 3 pegmatite, NW China, and its implications for the origin and tectonic setting of the pegmatite. Ore Geol Rev 32:325–336

Webber KL, Simmons WB, Falster AU, Foord FE (1999) Cooling rates and crystallization dynamics of shallow level pegmatite–aplite dikes, San Diego County, California. Am Mineral 84:708–717

Worku H (1996) Geodynamic development of the Adola Belt (southern Ethiopia) in the Neoproterozoic and its control an gold mineralization. Ph.D. thesis, Tech Univ Berlin, 156p

Worku H, Schandelmeier H (1996) Tectonic evolution of the Neoproterozoic Adola Belt of southern Ethiopia: evidence for a Wilson Cycle process and implications for oblique plate collision. Precambr Res 77:179–210

Yibas B, Reimold WU, Armstrong R, Koeberl C, Anhaeusser CR, Phillips D (2002) The tectonostratigraphy, granitoid geochronology and geological evolution of the Precambrian of southern Ethiopia. J Afr Earth Sci 34:57–84

Yibas B, Reimold WU, Anhaeusser CR, Koeberl C (2003) Geochemistry of the mafic rocks of the ophioloitic fold and thrust belts of southern Ethiopia: constraints on the tectonic regime during the Neoproterozoic (900–700 Ma). Precambr Res 121:157–183

Yihunie T (2002) Pan-African deformation in the basement of the Negele area, southern Ethiopia. Int J Earth Sci (Geol Rundsch) 91:922–933

Yihunie T (2003) Chemical Th–U–total Pb isochron ages of zircon and monazite from granitic rocks of the Negele area, southern Ethiopia. J Earth Planet Sci Nagoya Univ 50:1–12

Yihunie T, Adachi M, Takeuchi M (2004) P–T conditions of metamorphism of Neoproterozoic rocks of the Negele area, southern Ethiopia. Gondwana Res 7:489–500

Zerihun D (1991) Le mineralizzazioni a Ta-Nb: classificazione, prospezione, valutazione. Il caso di Kenticha (area di Adola, Sidamo—Ethiopia).—unpubl Ph.D. thesis, Univ of Milan, 365p

Zerihun D, Garbarino C, Valera R (1995) Granite pegmatite system in Kenticha (Adola, Sidamo, Ethiopia) rare metal pegmatite belt: petrochemistry, regional pegmatite zoning and classification. SINET Ethiopian J Sci 18:119–148